Transient rip currents and nearshore circulation on a swell-dominated beach

D. Johnson and C. Pattiaratchi
Centre for Water Research, University of Western Australia, Perth, Western Australia, Australia

Received 28 January 2003; revised 24 October 2003; accepted 18 November 2003; published 26 February 2004.

[1] Eulerian and Lagrangian measurements of nearshore circulation on a longshore uniform beach with perpendicularly incident swell waves are described. Both the Eulerian and Lagrangian data show a variable rotational part of the current field that is distinct from, but coexists with, that due to infragravity waves. A well-defined feature of the flow field includes transient rip currents, which occur in varying locations and are not topographically controlled. Drifter trajectories show that the rips behave like a shallow plane jet, consisting of a constrained neck region that flows into a spreading head region. There is continuous modulation of the flow within the rip neck. Estimates of the length scale across the rip neck using two-particle statistics are 20–30 m. Well-defined discrete vortex features are observed at the initiation point of one of the necks and in one of the rip heads. Estimated dispersion values suggest that mixing is greatly enhanced outside the surf zone by the intermittent presence of the rip heads. The dispersion calculated from both inside and outside the surf zone appears to show scale dependence with a power law close to 4/3 in a similar way to oceanic turbulence at much larger scales. *INDEX TERMS:* 4546 Oceanography: Physical: Nearshore processes; 4512 Oceanography: Physical: Currents; 4568 Oceanography: Physical: Turbulence, diffusion, and mixing processes; 4594 Oceanography: Physical: Instruments and techniques; *KEYWORDS:* rip currents, drifters, surf zone

Citation: Johnson, D., and C. Pattiaratchi (2004), Transient rip currents and nearshore circulation on a swell-dominated beach, *J. Geophys. Res.*, *109*, C02026, doi:10.1029/2003JC001798.

1. Introduction

[2] Rip currents are a generic name given to offshore directed flows which resemble plane jets with a strong constrained flow that broadens and forms a head region once it passes beyond the surf zone. The primary driving mechanisms for rip current circulation are believed to be longshore variations in the radiation stress gradient and setup. Detailed measurements of the forcing presented by *Haller et al.* [2002] show this to be the case as do model simulations which reproduce rip type circulations [*Haas et al.*, 1999]. Conservation of mass must also be satisfied, so that the offshore directed flow is balanced by an onshore flow which can be due to the wave induced flux (both from breaking and Stokes drift), or a diffuse onshore mean flow, or both.

[3] Longshore variation of the radiation stress gradient is caused by differential wave transformation in the longshore direction. This may be due to (1) topographic variation [*Bowen*, 1969], (2) spatial variability of the incident wave field due to wave groups [*Dalrymple*, 1975], (3) interaction of the incident wave field and the wave-averaged mean current [*Dalrymple and Lozano*, 1978; *LeBlond and Tang*, 1974; *Murray and Reydellet*, 2002], and (4) interaction of the incident wave field with lower-frequency waves such as edge waves [*Bowen*, 1969; *Sasaki and Horikawa*, 1978; *Symonds and Ranasinghe*, 2001]. The first mechanism leads to relatively fixed "topographic rips". On sandy beaches, the positions where rip channels occur are likely to be determined by some or all of the hydrodynamic mechanisms and subsequently reinforced by feedback between the hydrodynamics and sediment transport as proposed by [*Hino*, 1975]. There may be subsequent migration and morphological adjustment of these rip channels [*Brander*, 1999]. Attempts to predict rip spacing [*Hino*, 1975; *Short*, 1985; *Huntley and Short*, 1992] have produced inconclusive results and suggest that where rip channels chose to form may be due to complex interactions. Topographic rips often have a continuous mean offshore flow which may "pulse" strongly [*Cook*, 1969; *Bowman et al.*, 1988a, 1988b; *Aagaard et al.*, 1997].

[4] Rip currents can, in theory, occur on a longshore uniform beach without topographic control. The radiation stress field is spatially and temporally variable because of one of the latter three mechanisms above, leading to "transient rips" which occur in differing locations. Rip currents, which migrate in response to the variation of the incident wave field, are proposed as an alternative explanation for low-frequency oscillations attributed to shear waves [*Fowler and Dalrymple*, 1991]. While they have been generated in the laboratory [*Fowler and Dalrymple*, 1991], there is no conclusive proof that these transient type rips exist in the field and are completely unrelated to topography. Qualitative observation has been documented by *Vos* [1976] and *Tang and Dalrymple* [1989] measure

0148-0227/04/2003JC001798$09.00

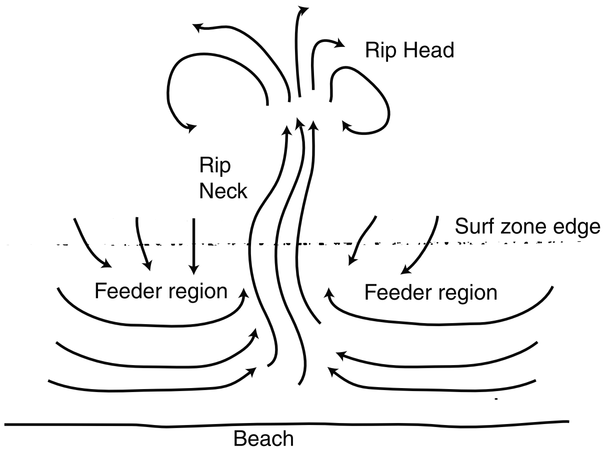

Figure 1. Schematic of the main features in rip current system.

migrating and pulsating rip currents, and note the nonstationary nature of the nearshore circulation system. *Murray et al.* [2004] present data of rip positions on a longshore uniform beach which do not show any preferred location. Another source of transient type rips has been observed in numerical model simulations of longshore currents, where shear wave instabilities are observed to produce jet-like currents which branch off the main flow and penetrate some distance offshore [*Allen et al.*, 1996; *Ozkan-Haller and Kirby*, 1999].

[5] Quantitative confirmation that transient rip position is entirely independent of topographic variation requires simultaneous measurement of topography and the flow field over a wide area, which is a formidable task. However, there seems to be sufficient indirect evidence for the existence of transient rip currents that can at least be said to not be "strongly" topographically controlled, and therefore distinct from rips which occur in well-defined rip channels. Transient rips are then, by definition, temporary features which develop in varying locations, have a specific lifetime and then decay.

[6] Once initiated, a rip current develops into a distinct current system consisting of three main features (Figure 1):

[7] 1. A feeder region where the currents are directed toward the center of the rip and provide the volume flux for the offshore flow. Numerical modeling experiments suggest that in topographic rips, the extent of the feeder region is largely independent of rip spacing and that the rip is only supplied by a small local area [*Svendsen et al.*, 2001]; whether this is the case in transient rips is not known.

[8] 2. The rip neck which is the narrow offshore flowing section of the rip which usually has the highest current velocities and may extend a significant distance outside the surf zone. This may be directed perpendicular or obliquely to the shore, may have a meandering shape and may move around.

[9] 3. The rip head, which is the seaward end of the rip current, is often clearly visible as a sediment laden patch of water at the end of the narrower neck. This patch of water may persist as a coherent feature for some time after the rip flow has ceased. Distinct vortex features are often seen in this region.

[10] While the exact arrangement in a rip system varies greatly, simple conservation of mass means that all rip currents must possess these three basic regions in some form.

[11] Previous field work has examined the spatial structure and dynamics of rip current flow with arrays of current meters [*Bowman et al.*, 1988a, 1988b; *Aagaard et al.*, 1997], Lagrangian measurements with drifters [*Shepard et al.*, 1941; *Shepard and Inman*, 1950; *Sonu*, 1972; *Sasaki and Horikawa*, 1975, 1978; *Brander and Short*, 2000; *Schmidt et al.*, 2003], dye tracer [*Sonu*, 1972; *Brander*, 1999], video observations [*Symonds et al.*, 1998], and side-scan sonar images [*Smith and Largier*, 1995]. While the existing data have provided a good general understanding of the main characteristics of rip currents and typical current velocities, detailed dynamics of rip currents in the field remain poorly understood.

[12] Rips and associated circulation cause spatial and temporal variation of the nearshore current field; however their length scales across the rip neck are much smaller than the typical length scales of long waves at frequencies less than the incident wave field (hereafter collectively referred to as infragravity waves). Rip currents are associated with freely evolving vortical flow, which *Peregrine* [1998] pointed out is distinct from irrotational flows associated with infragravity waves. Vortical structures in the nearshore zone, while acknowledged to exist, have received little attention in the field mainly because of difficulties in observing them.

[13] This paper presents field investigations of small-scale rip currents and the associated nearshore current structure on a medium energy swell-dominated beach using Lagrangian and Eulerian techniques. The aim of the experiments were to improve the understanding of detailed dynamics of the offshore directed flows, believed to be transient type rips and concentrates on variability over short time (10–1000 s) and space (10–100 m) scales.

2. Field Site and Methodology

2.1. Field Site

[14] The field measurements were carried out on three days during (Southern Hemisphere) winter between 5 July and 20 September 2001, on Leighton beach, one of the metropolitan beaches in Perth, Western Australia. The site experiences diurnal microtidal tides with a mean spring tidal range of 0.6 m. Offshore reefs and islands significantly reduce the offshore swell height so that Leighton beach experiences low to moderate energy conditions with significant wave heights typically between 0.5 m and 1.2 m in winter. Weather conditions are dominated by the passage of fronts with onshore winds and locally generated seas separated by periods of predominantly offshore winds and a swell-dominated wave climate. The beach undergoes rapid adjustment in response to the wave climate with erosion occurring during the passage of fronts followed by accretion during the swell-dominated calm periods [*Masselink and Pattiaratchi*, 2002]. The formation of a bar sometimes occurs at the field site in response to continued storm activity. However, in 2001, storm conditions were relatively mild and a fixed bar feature did not develop. The dates of the experiments were 5 July (experiment 1), 13 September

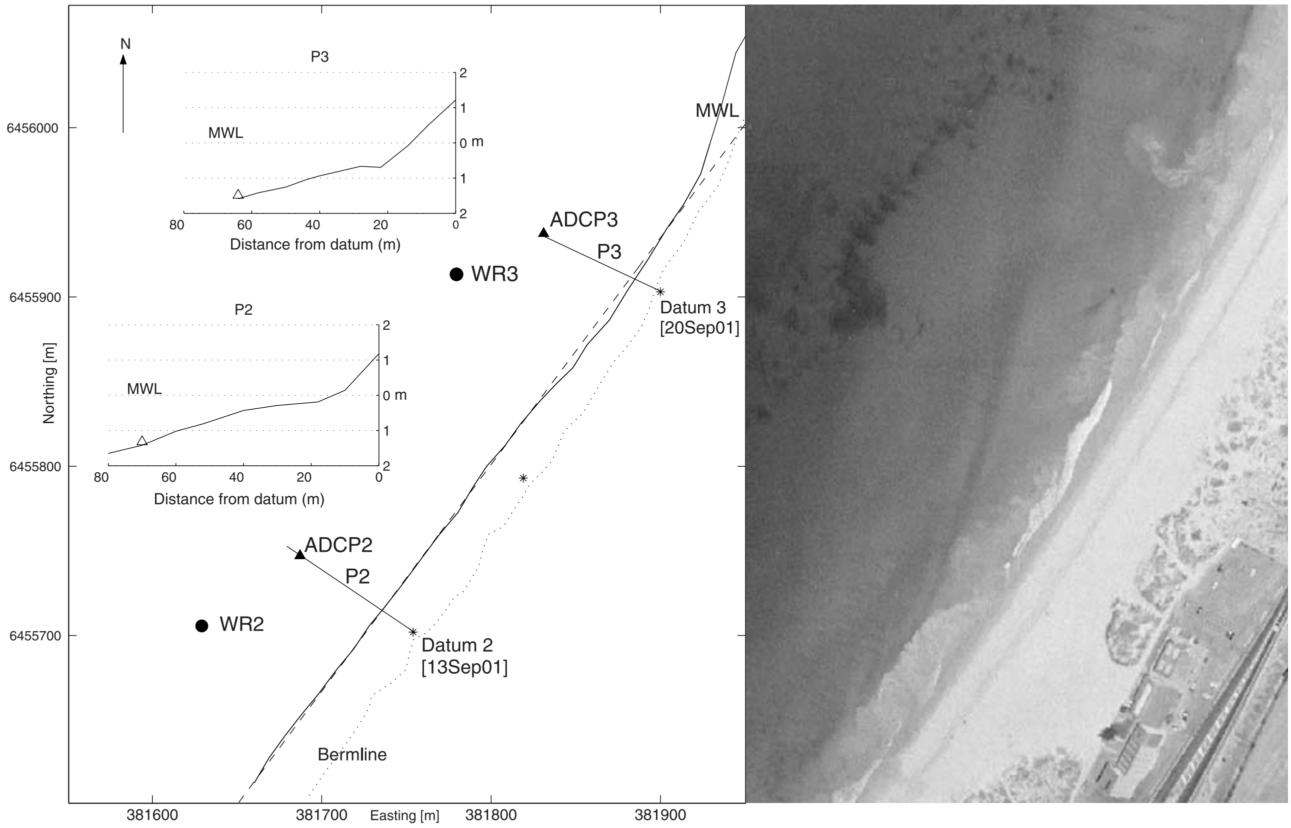

Figure 2. Plan of instrument deployment with aerial view of the field site. ADCP and wave recorder (WR) indicate positions of the instruments for the second and third experiments. Lines from the datum points show profile transect lines (P2 and P3). Mean water level (MWL) in plan view is mapped by walking with a GPS unit. MWL in beach profiles calculated from mean depth of water at the ADCP position. Dashed line is the best fit line of the shoreline used for the rotation of the coordinate axes for cross-shore and longshore orientation.

(experiment 2), and 20 September (experiment 3). Conditions for the experiments were chosen to be swell-dominated. On the days of the measurements, the winds were offshore (from the NE) and hence there were no locally generated wind waves incident at the site.

2.2. Field Methodology

[15] Instrumentation consisted of a wave recorder, an upward looking acoustic Doppler current profiler (ADCP) and four drifters with Global Positioning System (GPS) receivers. The positions of instrument deployments are shown in Figure 2. The aerial photograph is of the same area although not taken at the same time; note the rip current at the northern end of the beach. For experiment 1 only the drifters were used. The drifters themselves are discussed in more detail in section 2.3 below.

[16] The wave recorder was a FSI Microtide set to sample pressure at 4 Hz. This was deployed in around 2.5 m depth on a weighted disk on the seabed approximately 30 m seaward of the outer limit of wave breaking. The ADCP was a Nortek Aquadopp Profiler set to sample 0.1 m bins at 1 Hz. The instrument features a sensor head a right angles to the main body so that the upper surface of the sensor can be positioned very close to the seabed. The instrument was mounted flush on a cross shaped frame which, because of its low profile, is fixed and stable even when directly below breaking waves. The upper surface of the sensor was 0.05 m above the bed and with a blanking distance of 0.2 m this put the center of the lowest bin at 0.3 m above the bed. The instrument was deployed just inside the breaker line.

[17] Nearshore profiles were surveyed using a theodolite. The GPS receiver units were used to fix the instrument positions and survey the beach face by walking the bermline and the approximate MWL. A line of best fit was drawn along the MWL line and for subsequent analysis, the coordinate system rotated and translated to on/offshore and longshore axes with the longshore axis coincident with the best fit MWL line. The approximate position of the outer limit of the surf zone in each experiment was estimated visually relative to a fixed buoy (located with a GPS unit). The SE (cross-shore) and NE (longshore) directions are defined as positive x and y respectively, and x is measured from the MWL line. All position and velocity data is presented with respect to this rotated coordinate system.

2.3. Surf Zone GPS Drifters

[18] The drifters were newly developed GPS tracked drifter units [*Johnson et al.*, 2004], which are suitable for use in the surf zone. The drifters are compact receiver units attached to a series of one or more parachutes as shown in Figure 3. An internal datalogger records Longitude/Latitude

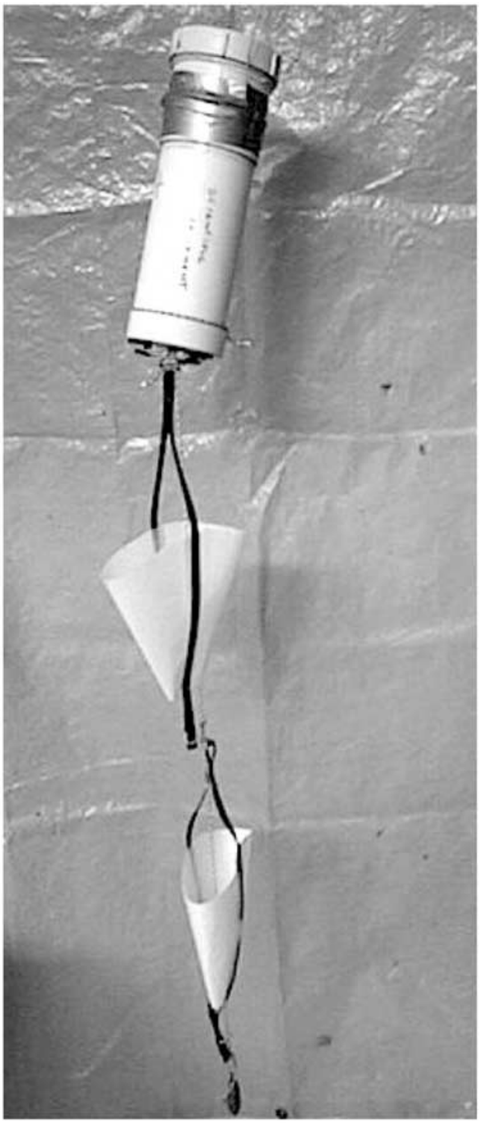

Figure 3. Surf zone GPS drifter with two parachutes. The receiver unit is the cylinder at the top of the assembly, which has a total length of 30 cm.

fixes from an integrated GPS antenna/receiver at 1 Hz. The parachutes act to prevent the drifter body from surfing on the faces of broken waves and effectively anchor the drifter assembly to the deeper orbital velocities. Although sometimes completely submerged in breaking waves, data recovery is better than 99%. The drifters were deployed and recovered by hand. Similar instruments are also described by *Schmidt et al.* [2003] but use a different approach to damp surfing.

[19] The raw position data from the drifters was converted to Universal Transverse Mercator (UTM) coordinates and filtered with a fifth-order Butterworth filter with a low-pass cutoff of 0.05 Hz. A processing function was used which convolves the filter kernel both ways through the raw data to ensure a zero phase response and includes an algorithm to minimize end effects. Filtering has the dual effect of removing high-frequency position errors and averaging the incident wave motion. Velocities were calculated by centered differences from the filtered trajectories. A criteria of an onshore movement exceeding 1.7 m s^{-1}, the approximate phase speed of waves in the minimum operating depth, was used to flag occasional surfing events and these datum points and datum points 10 s before and after (the same width as the filtering window) were excluded from any quantitative analysis.

[20] The accuracy of the instrument is determined by two separate factors. The first is the positioning accuracy of the receiver unit. This can be estimated by examining the fluctuation in apparent position of a stationary receiver and is described by *Johnson et al.* [2004]. For a 45 min test, the standard deviation of position from the mean was 1.3 m in the easting direction and 1.6 m in the northing direction. Maximum displacements from the mean position were 4.2 and 5.2 m. The spectral density of the GPS position error spectrum is less than 10% of a typical surf zone Lagrangian velocity spectra for frequencies below 0.05 Hz.

[21] The second factor is what exactly the drifters actually measure in terms of local hydrodynamic variables. An analysis of the drifter performance, in terms of their dynamic response and positioning, is quite long and is addressed by *Johnson and Pattiaratchi* [2003]. The key results of the instrument validation are summarized below. Of interest is whether the wave-averaged drifter velocity, $\mathbf{V}(\mathbf{r}, t)$ at a wave-averaged position $\mathbf{r}$ is a good estimate of the depth and wave-averaged Eulerian velocity $\bar{\mathbf{u}}(\mathbf{r}, t)$ so that

$$\mathbf{V}(\mathbf{r},t) \simeq \bar{\mathbf{u}}(\mathbf{r},t) = \frac{1}{Td}\int_{t-T/2}^{t+T/2}\int_{-h}^{\eta}\mathbf{u}(\mathbf{r},z,t')\,dz\,dt', \qquad (1)$$

where $\mathbf{u}$ is the (depth-dependent) instantaneous velocity, as for example, measured with the ADCP. η is the surface elevation, h is the depth below static water level (SWL), d is the total water depth, $d = \overline{\eta} + h$ (the overbar indicates time averaging). Equation (1) is the usual definition of wave-averaged currents, and for monochromatic waves, T is the wave period. Without a single well-defined wave period, as is the case in real sea states, the time integral can be viewed as equivalent to a boxcar filter with low-pass cutoff of $1/T$. In practice we use a Butterworth filter (that has better response characteristics) with low-pass cutoff of 0.05 Hz which corresponds to $T = 20$ s in a conceptual sense. The cutoff frequency of 0.05 Hz is the lower limit of the frequency band of incident wave motion. In discussion of data, the term wave-averaged refers to filtered data.

[22] A field experiment compared filtered drifter velocities with depth averaged and filtered ADCP measurements by repeatedly deploying a drifter in the vicinity of the ADCP. Results from 53 deployments are shown in Table 1; while there is a significant amount of scatter in the data points (mainly because of the practical difficulties of the validation procedure), the lines of best fit show that equation (1) is a reasonable assumption. The drifters appear to move slightly slower than the Eulerian wave and depth-averaged velocity, although in the longshore case with a fixed zero intercept the agreement is very close. The low R^2 values and high standard deviations reflect the scatter in the data, however the best fit agreement is remarkably good,

Table 1. Summary Statistics for Comparison of Drifter Wave-Averaged Velocities With Depth and Wave-Averaged ADCP Velocities[a]

	M	I, m s^{-1}	R^2	M_{fix}	σ, m s^{-1}
Cross-shore	0.85	−0.02	0.59	0.91	0.16
Longshore	0.94	0.02	0.57	1.02	0.14

[a] M, I, and R^2 are the gradient, intercept, and r squared values from a linear regression of the drifter velocity against ADCP velocity, $V_{(drifter)} = M.\bar{u}_{(ADCP)} + I$. The M_{fix} is a gradient for a linear regression with forced zero intercept. CC is the correlation coefficient for the two measurements, and σ is the standard deviation of the difference between the measurements, $V_{(drifter)} - \bar{u}_{(ADCP)}$.

especially in the cross-shore direction (where the effect of wave breaking should be most significant).

[23] Data from 14 deployments of three or four drifters are used in this paper. Each deployment was started in a rip neck (Figure 1) by releasing the drifters simultaneously at the same place once the rip current was observed to have been initiated. A deployment was terminated once all drifters were outside the surf zone and observed to be almost stationary or until one of the drifters beached on the shore.

3. Eulerian Measurements

3.1. Wave Recorder

[24] Spectra calculated for the periods spanning the drifter deployments on each day are shown in Figure 4. The spectra were calculated from a set of overlapping sections of 512 s (2048 data points) data segments which were linearly detrended and tapered using a Hanning window with the final spectra an average of the set of Fourier transformations. Pressure data from the wave recorder were used for experiment 2 and experiment 3. For experiment 1, data from a wave rider 2 km to the north west of the field site was used. Corresponding to visual observations, the spectra indicate a narrow banded swell-dominated sea on all three days. Significant wave heights were calculated as $H_s = 4\sqrt{(M_o)}$, where M_o is the zeroth spectral moment and were 1.02, 0.79, and 1.03 m for the three experiments. While the calculated H_s is larger during experiment 1 than experiment 2, this data was from an offshore source and included some locally generated waves; visual estimates of wave height were similar to experiment 2.

[25] The tidal influence during the measurement periods was very small. The mean water level measured by the wave recorder, defined here as the water level component passing a 0.0001 Hz filter, showed virtually no change for experiment 2 and a 10 cm variation for experiment 3 with high tide occurring at around 1330. While there is no direct tidal measurement for experiment 1, the tidal predictions for Fremantle 2 km to the south indicate a tidal rise of only 0.18 m between 1121(LW) and 1939(HW) which spanned the period of the measurements. The aim was to collect data under very similar hydrodynamic conditions so that some generic conclusions about the hydrodynamic regime under narrow banded swell-dominated conditions can be made.

3.2. ADCP

[26] Three hour mean ADCP data spanning the period of deployments on each day are shown in Figure 5. The measured current in any bins above the instantaneous measured water level were set to zero. The mean water level was determined from the instrument pressure sensor data assuming hydrostatic pressure; this procedure will tend to slightly underestimate the water (or rather air-foam interface) level under the crest of breaking waves because of bubbles and a decreased pressure due to strong vertical accelerations. The mean current velocities are low but exhibit a classic undertow profile with onshore flow at the mean water level and offshore flow in the lower part of the water column. Below the level of transition between

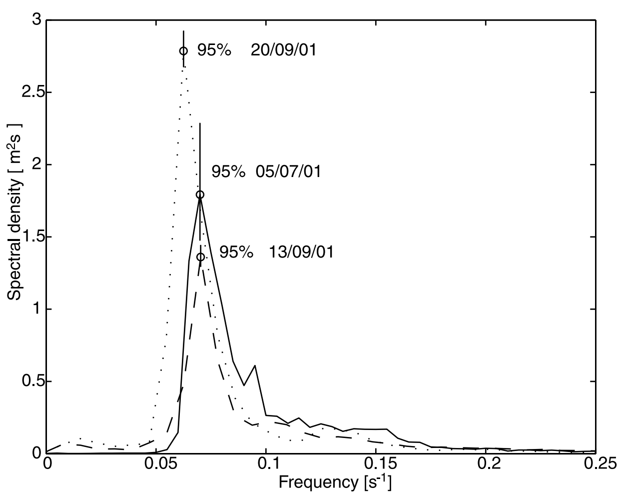

Figure 4. Spectra calculated from an offshore wave buoy data from experiment 1 (5 July, solid line) and the wave recorder data from experiment 2 (13 September, dashed line) and experiment 3 (20 September, dotted line).

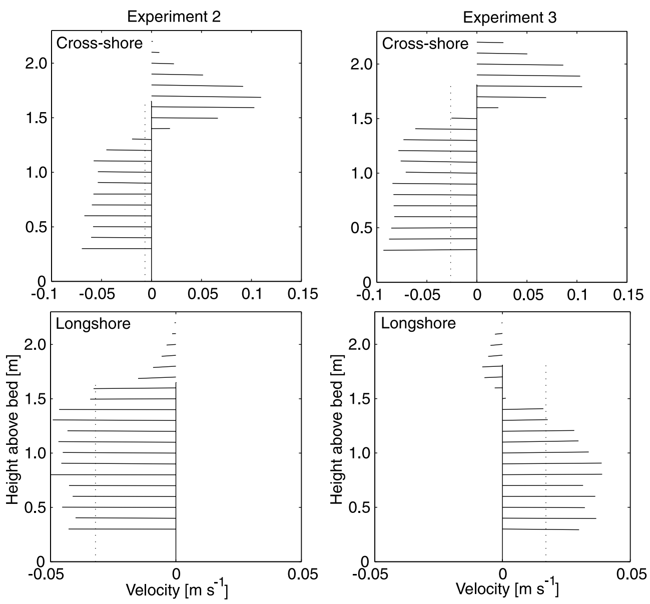

Figure 5. Three hour means of ADCP data of cross-shore and longshore velocity for experiment 2 and experiment 3. The cross-shore and longshore velocity components are shown for each depth bin. The height of the solid vertical line corresponds to the mean depth. The depth-averaged velocity is indicated with a dotted line.

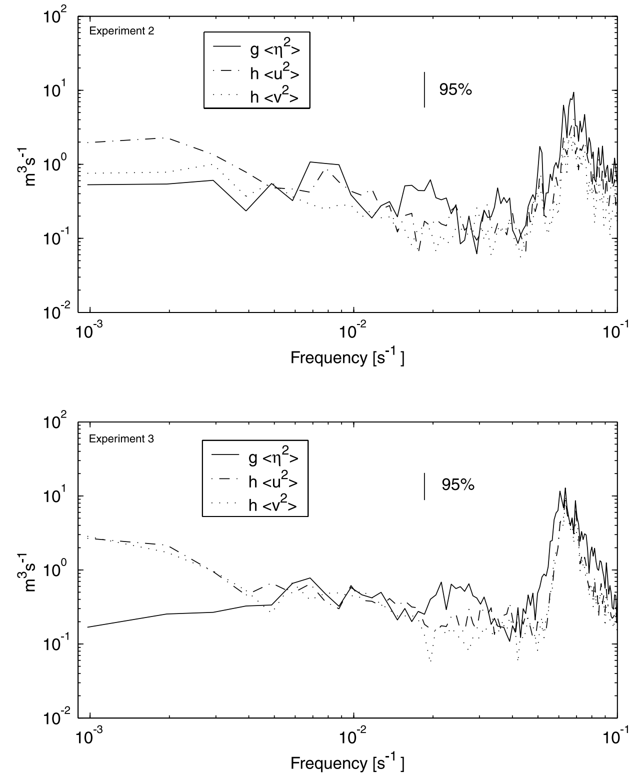

Figure 6. Spectra of pressure and depth-averaged velocity from 3 hours of ADCP measurements spanning the period of drifter deployments for (top) experiment 2 and (bottom) experiment 3. The spectral density of the current components and surface elevation has been multiplied by the mean depth, h, and gravitational acceleration, g, respectively, so that they correspond to estimates of potential and kinetic energy contributions. Note that the spectra are not variance preserving.

onshore and offshore flow, there is little vertical variation with depth. The higher cross-shore current magnitudes for experiment 3 are due to the larger wave heights on this day. The longshore current is in different directions on the two days and shows greater vertical variation for experiment 3. Depth-averaged flow velocities are small and directed offshore in both cases but in different longshore directions.

[27] Figure 6 shows spectra, calculated as for the wave recorder with overlapping sections of 1024 s (1024 datapoints), of the ADCP pressure and depth-averaged velocity for same three hour sections of experiment 2 and experiment 3 as used for the means shown in Figure 5. To characterize the low-frequency flow climate during the experiments, we estimate ratios of kinetic and potential energy using the method of *Lippmann et al.* [1999]. The ratio is defined in terms of variances of velocities and surface elevation:

$$R = \frac{h\left(\langle u^2 \rangle + \langle v^2 \rangle\right)}{g\langle \eta^2 \rangle}, \tag{2}$$

where u, v, η are depth averaged velocities and pressure at the ADCP. Variances are calculated by integrating the spectra in Figure 6 in the range $f = 0.0025-0.05$ Hz. Values of R are 1.29 for experiment 2 and 1.57 for experiment 3. A ratio of 1 would correspond to an equipartition of kinetic and potential energy consistent with gravity wave modes while for nondivergent motions $R \gg 1$. The estimated values indicate that there is a significant amount of energy, 22% and 36% respectively, not associated with free infragravity wave modes. As expected from the relative increase of the current variance at lower frequencies in the spectra, the ratios increase as the frequency band is shifted to $f = 0.0025-0.01$ Hz where the ratios are 1.78(43%) and 2.86(65%). It is worth noting that estimates of noninfragravity energy due shear waves using equation (2) were found to be biased high by *Noyes et al.* [2002] when compared to methods based on longshore current meter arrays. Nevertheless, the important implication of the ratios is that while the current variance is dominated by infragravity motion, there is a significant other mode of nearshore current variability present.

4. Descriptive Analysis of the Rip Currents

[28] Four of the rip events are discussed and analyzed in more detail in what follows. The individual plots are all rotated to the on/offshore coordinate system. The four rip events were chosen because they represent the two main types of rip flow observed. In addition, in these deployments the drifters, which were deployed in a cluster, remained in the rip neck in each case; this is beneficial for quantitative analysis described in section 5. The duration of the data presented for each event is 800 s except for RE2a which lasts for 1800 s. The first two rip events, RE3a and RE3b shown are from experiment 3 and both show "classic" rip currents flowing almost directly offshore. Visual observations were of very well defined rips occurring in different locations approximately every 5 min. The third and fourth rips, RE2a and RE2b, are from experiment 2 where the rips were less well defined, flowed obliquely to the shore and appeared for a longer duration. The reasons for the difference in rip flow between experiment 2 and experiment 3 are not clear. The records from the wave recorder for the periods of the four rip events are shown in Figure 7. The incident wave field has a smaller significant wave height and is less groupy in experiment 2 than in experiment 3. There may also be an associated difference in the directional characteristics of the wave field, but no data is available to investigate this.

[29] During experiment 2, the drifters also moved back onshore relatively quickly, so it was practical to leave them to complete a circuit of the rip current circulation and flow back out in a second rip that subsequently developed. In contrast, the rips in experiment 3 moved the drifters further and more directly offshore, from where they moved onshore very slowly; for practical reasons (to conduct more than one deployment per day) the drifters were recovered before they completed a circuit of the circulation system. The rip events during experiment 1 were very similar in nature to those in experiment 3 with narrow, well-defined necks perpendicular to the shore. In experiment 1 all drifters tended to move longshore toward the south after moving offshore in the rips, indicating there was some continuous longshore current, however there is no current meter data from this day to corroborate this. Data from this day are not discussed in

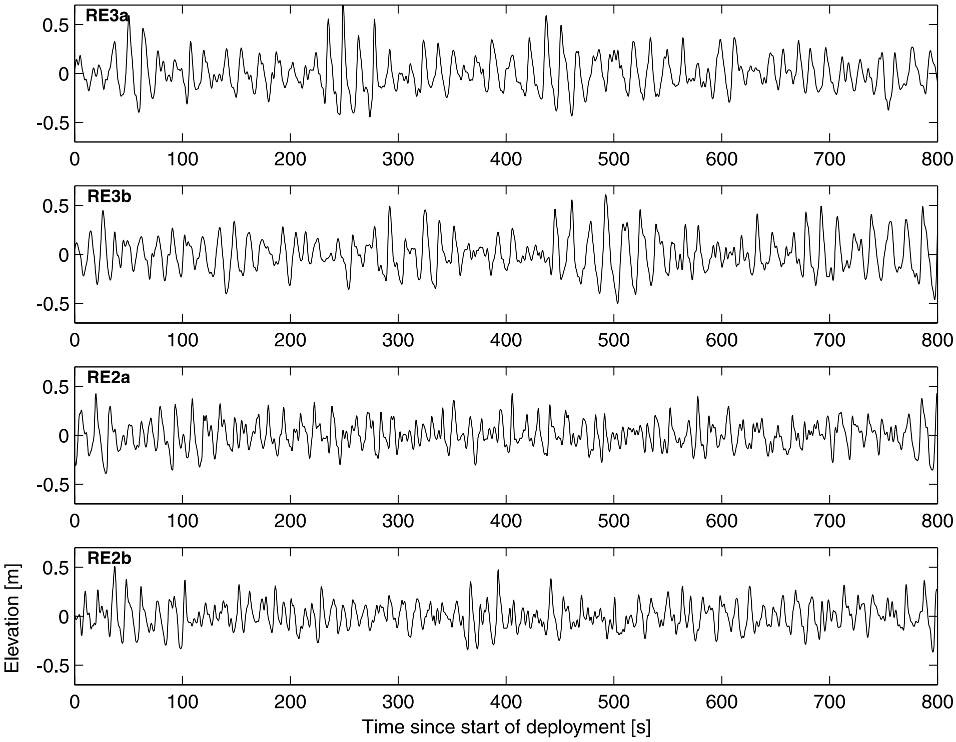

Figure 7. Wave records from the wave recorder for the duration spanning the rip events except for RE2a where only the first 800 s are shown.

detail but are included in the analysis of relative dispersion and length scales.

4.1. Rip Event 3a

[30] The trajectories show a well-defined offshore flow which appears to spread and dissipate outside the surf zone (Figure 8). A "classic" rip current neck and head region can be seen. The trajectories show all the characteristics of a plane jet being ejected from the surf zone. There is little longshore spreading in the neck section indicating a constrained jet-like flow, while in the head the drifters rapidly spread, consistent with the visually observed mushroom shape at the offshore limit. For the first 120 s (subplot a) flow is strongly offshore with instantaneous velocities up to 1.1 m s^{-1} and an average speed of 0.5 m s^{-1}. There is significant variability within a very narrow section, with two of the drifters turning shoreward in a meander while the others are not affected. At 120 s (subplot b) two of the drifters almost stop while the other two continue moving offshore, again showing significant variability over a very short distance. One drifter ends up outside the jet region and is left behind, indicating very little offshore flow outside of a tightly constrained region. Once 100–110 m offshore, the trajectories spread out with the outer two drifters turning back shoreward. Drifter velocities decelerate rapidly in the head region; at around 300 s (subplot c), now some 100 m offshore, the drifters are almost stationary.

[31] The spatial gradients of the velocities across the rip neck and the diverging region of the head are strong; the ADCP measurements (not shown), from 20 m alongshore show some mean offshore flow as the drifters pass, but less than half the average velocity of the drifters, indicating the region of strong offshore flow is tightly constrained.

4.2. Rip Event 3b

[32] The general features of this rip current are similar to RE3a (Figure 9). Again there is a well-defined neck region and a head region. For 60 s after deployment (subplot a) all drifters move offshore with peak speeds of 0.7 m s^{-1} and a mean speed of 0.5 m s^{-1}. After moving offshore initially, the trajectories of two drifters is interrupted by a surfing event and the trajectory of the third turns shoreward again. Between 110 and 200 s (subplot b) all the drifters turn back toward shore at some point and one has a net motion shoreward over this period. It appears that the rip flow is retarded and then pulses a second time, carrying the drifters well outside the surf zone. The fact that two of the drifters are surfing indicates the presence of particularly large breaking waves which would provide a strong local forcing in the shoreward direction. From 200 to 300 s (subplot c) all drifters move offshore in a well-defined rip neck with mean speed of 0.4 m s^{-1} and peak speed up to 1.0 m s^{-1}. After 300 s the flow begins to spread and the outer two drifters turn back shoreward. As with RE3a, the trajectories diverge in the head region although the flow patterns are more complex.

[33] One drifter describes almost two complete rotations in what appears to be a well-defined vortex structure. An estimate of the rotation rate of the first loop is 0.01 s^{-1}, while for the second it is 0.0025 s^{-1} indicating that the eddy is spinning down. Elliptical orbits of this type can be caused by mode 0 edge waves, which have circular horizontal particle orbits. However, the edge wave amplitudes required

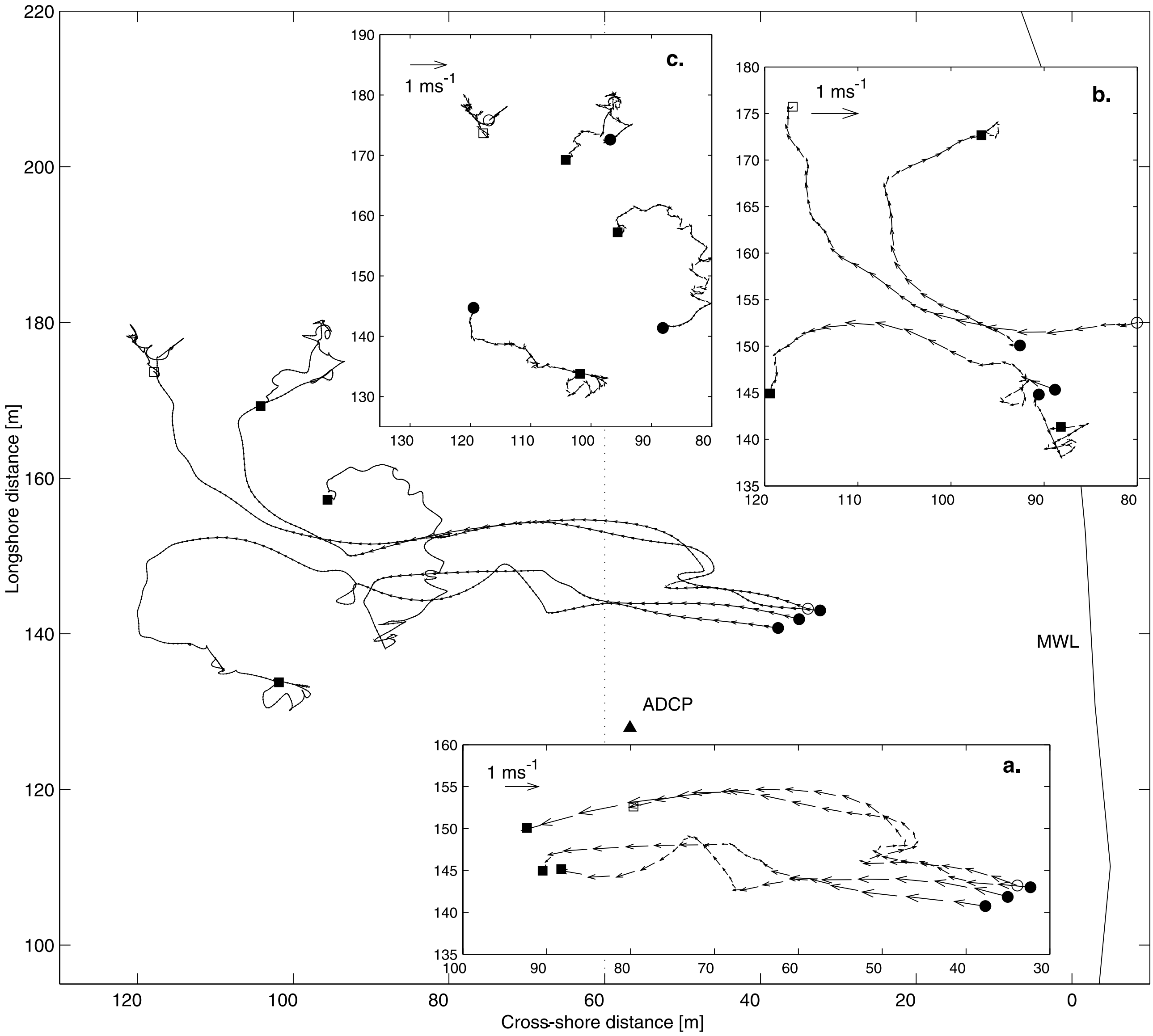

Figure 8. Velocity vectors for rip event 3a. The vector arrows are plotted at 5 s intervals. The main plot shows the tracks from the whole deployment, while the subplots show shorter sections: (a) T = 1–120 s, (b) T = 121–300 s, and (c) T = 301–800 s. Circles indicate the start of each segment, and squares indicate the end. The approximate outer limit of the surf zone is indicated in the main plot with a dotted line, and the position of the ADCP is indicated with a solid triangle.

to generate the observed orbital excursions, about 0.3 m at the ADCP and 0.2 m at the wave recorder, are not present in the surface elevation records.

[34] The ADCP measurements during the rip (Figure 10), from about 20 m alongshore, show almost no indication of the rip, supporting the visual observation of a narrow region of offshore flow. However, sustained offshore flow was recorded by the ADCP 480–660 s after the deployment of the drifters. This is most likely another rip occurring later at the ADCP position; an offshore flow of this magnitude and duration which was homogeneous longshore would completely drain the surf zone. There is little variation of the current strength below the flow reversal centered around mean water level and the shape of the undertow profile is apparently maintained and shifted toward negative (offshore) velocities. The rip seen in the ADCP data is initially shore perpendicular then swings to become oblique to the shore at the ADCP location.

4.3. Rip Event 2a

[35] This rip event has a different kind of structure from RE3a and RE3b (Figure 11). The offshore flow is oblique to the shore following a reversal at the initiation of the rip. All the drifters initially move directly offshore for about 50 s before turning shoreward again (subplot a). Speeds in both directions peak at about 0.7 m s^{-1}. At about 100 s all drifters then move obliquely offshore northward, with mean current speeds of 0.55 m s^{-1} and peak speeds of 0.9 m s^{-1} during the following 100 s. Once outside the surf zone the drifters turn shoreward and mean speeds slow to 0.2 m s^{-1},

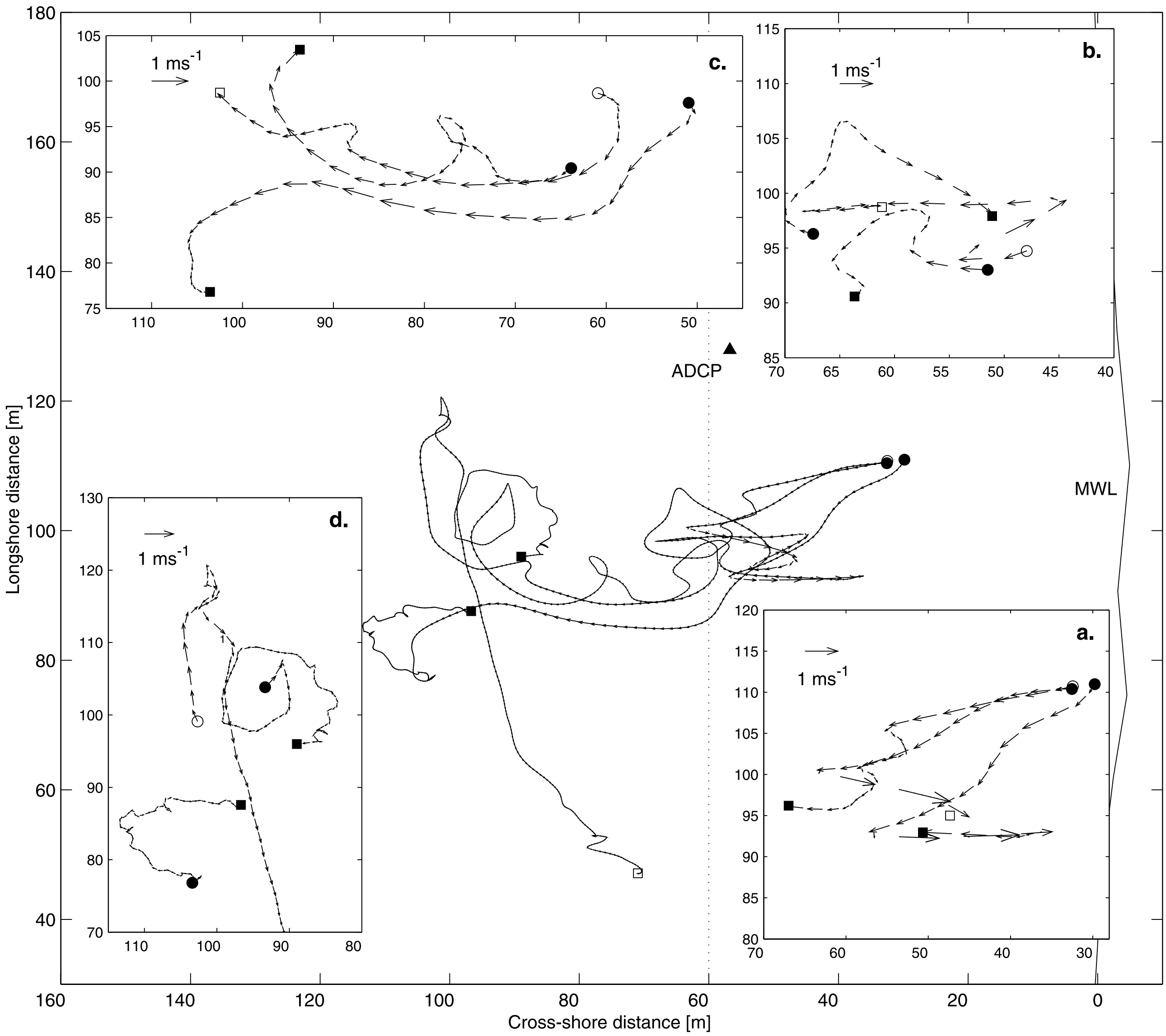

Figure 9. Velocity vectors for rip event 3b. The vector arrows are plotted at 5 s intervals. The main plot shows the tracks from the whole deployment, while the subplots show shorter sections: (a) T = 1–110 s, (b) T = 111–200 s, (c) T = 201–360 s, and (d) T = 361–800 s. Circles indicate the start of each segment, and squares indicate the end. The approximate outer limit of the surf zone is indicated in the main plot with a dotted line, and the position of the ADCP is indicated with a solid triangle.

but they remain in a constrained cluster and do not spread here. The flow then appears to become unsteady and meanders increasingly with the trajectories becoming less coherent (subplot b). Eventually the drifters split at around 600 s (subplot c) with two describing large looping trajectories rotating in opposite directions. The trajectories appear to describe a rip current which undergoes a large meander while still a coherent jet before spreading in a head type feature; note the qualitative similarity with the rip shown in the photograph of the field site (Figure 2).

[36] Two of the drifters subsequently move back well inside the surf zone. One of these does so in a surfing event while the other drifts back in a large loop with a mean speed of 0.1 m s^{-1}, presumably because of the net onshore flow which must be present. Both then appear, at different times, to be caught in a second rip event that transports them back offshore again this time in an obliquely south longshore direction with speeds peaking at 0.7 m s^{-1} (subplot d). These two drifters follow the type of trajectories expected in a complete rip current cell where a diffuse onshore flow in the feeder region supplies the rip necks. This general circulation appears to be present even though the rips themselves are apparently transient in time and space.

[37] As the drifter passes near the ADCP about 360 s after deployment, offshore and longshore flow is seen in the ADCP data, presented in Figure 10. Significant offshore mean flow occurs for two 60 s averaging periods and northward longshore flow persists for longer. Prior to this there is little mean flow, indicating a transient phenomena. Note that the direction of the rip flow is also in the opposite direction to the long time mean flow shown in Figure 5.

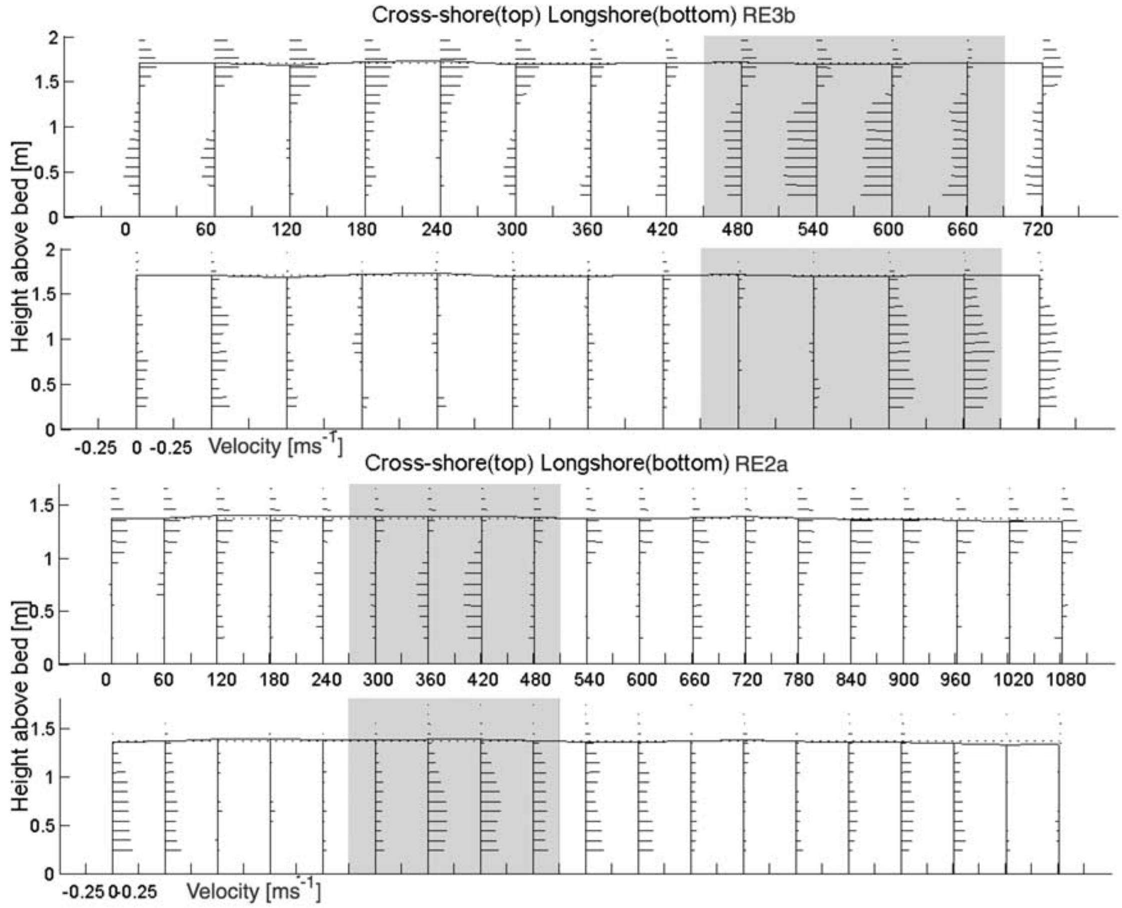

Figure 10. ADCP profiles during rip events 2 and 3. Velocities and water depth are averaged in 120 s blocks centered around the time indicated below each profile. The vertical bins have also been averaged with the adjacent bins in each case. The shaded areas in each case highlight periods of sustained offshore flow consistent with a rip current.

Again, here, ADCP data indicate little variation of horizontal velocity with depth.

4.4. Rip Event 2b

[38] An oblique rip current is observed (Figure 12) that shares several features with RE2a. First there is the initial reversal of direction, in what appears to be an eddy structure (subplot a) with mean speed of 0.3 m s^{-1} and a rotation rate of about 0.006 s^{-1}. As in section 4.2 the edge wave required to generate an orbit of this kind is not seen in the elevation records. Following this, all drifters move obliquely offshore with mean speed of 0.4 m s^{-1} and peak speeds of 0.9 m s^{-1}, the flow again becoming increasingly unsteady with distance. However, unlike RE2a, there is no significant large-scale meander in this case. Once outside the surf zone, the trajectories diverge and there is a reversal of direction with all drifters moving back inshore in the opposite alongshore direction from the initial rip. One of the drifters surfs inshore and subsequently moves offshore again, presumably into another rip current, this time oriented obliquely in the opposite longshore direction.

[39] Note that although RE2a and RE2b are similar in their shape and may appear to be constrained by the same topography, this rip event occurs 60 m longshore from RE2a. This distance is the same scale as the width of the surf zone so it seems unlikely that this can be due to a topographic rip channel. The latter stages of RE2a (around 1200 s) show drifters in the same region as the initial section of this rip event but moving in the opposite longshore direction. In addition, while RE2a and RE2b are immediately either side of the ADCP position, the depth-averaged longshore velocity as measured by the ADCP is in fact toward the south, in the opposite direction to the two rip events. If RE2a and RE2b were manifestations of the same topographic rip, this should be seen in the long time average current measured by the ADCP.

5. Analysis of Drifter Clusters

[40] The position of the centroids and the area spanned by simultaneous drifter positions or "clusters" are shown in Figure 13. The position of the cluster centroid, x_o, y_o is given by

$$x_o(t) = \frac{1}{n}\sum_{i=1}^{n} x_i(t) \quad y_o(t) = \frac{1}{n}\sum_{i=1}^{n} y_i(t), \tag{3}$$

where x_i, y_i is the position of one of n individual drifters. The velocity of the cluster is the rate of change of x_o, y_o

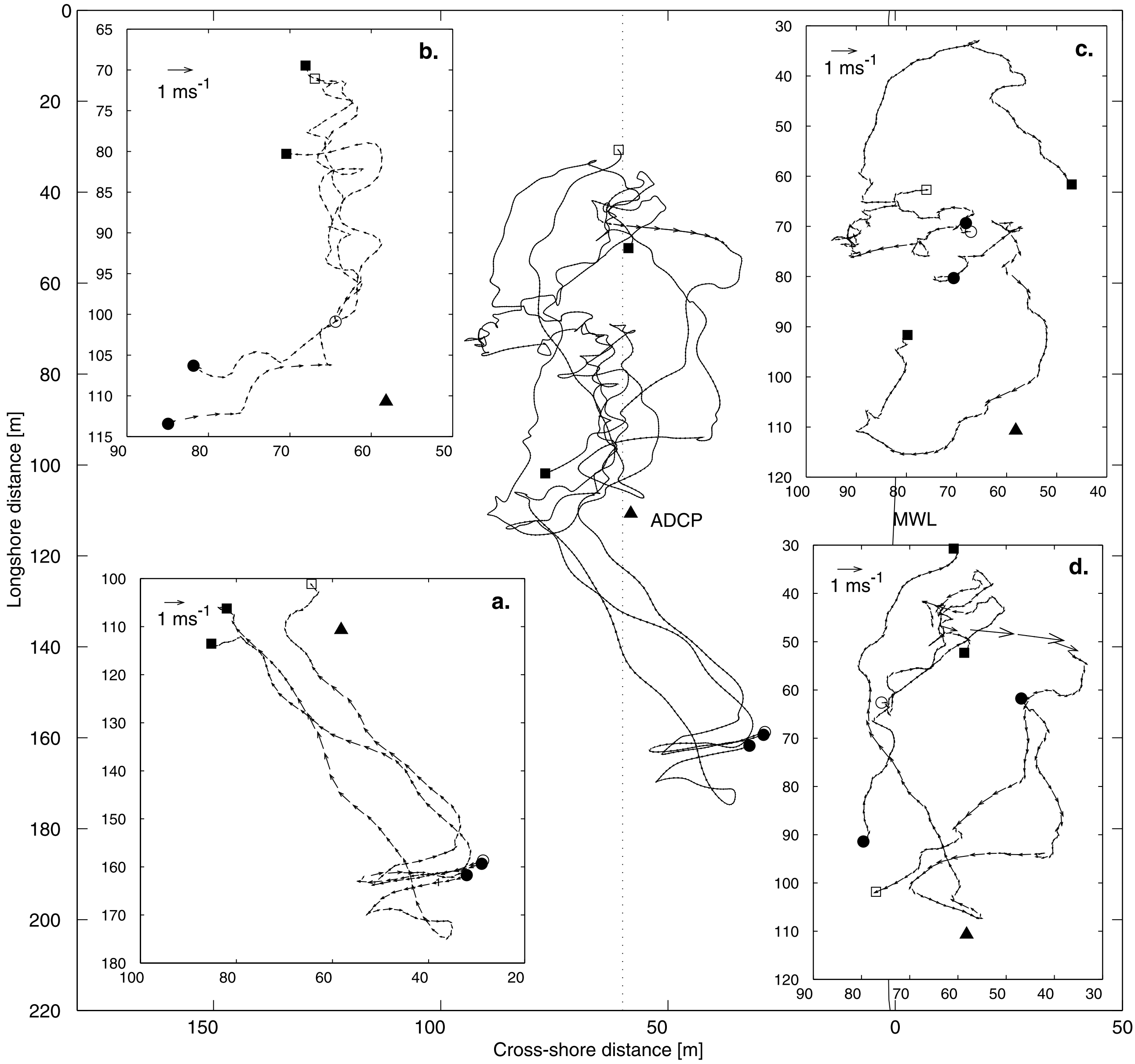

Figure 11. Velocity vectors for rip event 2a. The vector arrows are plotted at 5 s intervals. The main plot shows the tracks from the whole deployment, while the subplots show shorter sections: (a) T = 1–300 s, (b) T = 301–600 s, (c) T = 601–1200 s, and (d) T = 1201–1800 s. Circles indicate the start of each segment, and squares indicate the end. The approximate outer limit of the surf zone is indicated in the main plot with a dotted line, and the position of the ADCP is indicated with a solid triangle.

calculated by centered differences and is equivalent to the mean of the individual drifter velocities. The velocities of the cluster centroids are shown in Figure 14. In each case, the approximate time when the cluster centroid crossed the edge of the surf zone, and the time at which the rip neck ended, are shown. In addition, periods where one of the drifters is caught in a surfing event is indicated by a shaded region. While the net movement is offshore, there are significant fluctuations and changes in the on/offshore direction. In general, as would be expected, velocities are higher inside the surf zone and in the rip neck. Means, minimums (maximum offshore directed), maximums, and standard deviation of the velocity records from the rip neck section are shown in Table 2.

5.1. Dynamics of the Clusters in the Rip Neck

[41] The acceleration of a fluid column (or to be more precise, a volume spanning the water depth which moves at the depth-averaged velocity) is governed by

$$\frac{D\bar{\mathbf{u}}}{Dt} = -g\nabla\bar{\eta} + \frac{1}{\rho d}[\mathbf{F} + \mathbf{M} + \mathbf{B}], \qquad (4)$$

where $\bar{\mathbf{u}}$ is the current as defined in equation (1). The term $\mathbf{F}$ is the forcing due to wave motions with frequencies greater

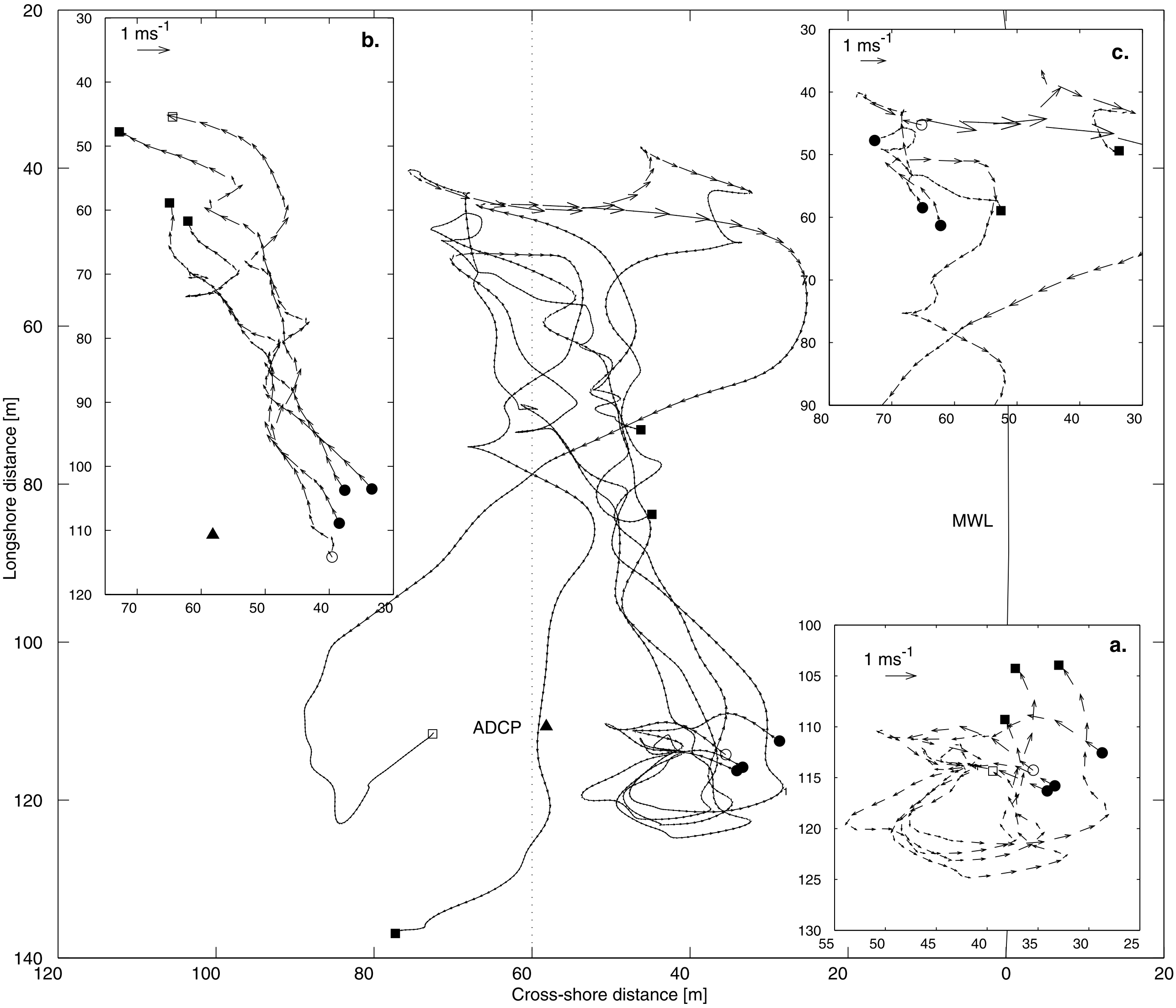

Figure 12. Velocity vectors for rip event 2b. The vector arrows are plotted at 5 s intervals. The main plot shows the tracks from the whole deployment, while the subplots show shorter sections: (a) T = 1–200 s, (b) T = 201–400 s, and (c) T = 401–600 s. Circles indicate the start of each segment, and squares indicate the end. The approximate outer limit of the surf zone is indicated in the main plot with a dotted line, and the position of the ADCP is indicated with a solid triangle.

than 0.05 Hz; this is not the same as the classic radiation stress, because of the random nature of the wave field. **M** contains all of the lateral momentum mixing (including shear dispersion mechanism [*Svendsen and Putrevu*, 1994]), and **B** is the bottom shear stress. Surface stresses due to wind have been neglected. This is essentially a shallow water equation with terms for the forcing and mixing due to the incident waves.

[42] Assuming that the drifters move with a velocity close to $\bar{\mathbf{u}}$ as expressed in equation (1), the mean forcing acting across the cluster equals the acceleration of the centroid. By considering clusters, the forcing is occurring over the same length scale as the cluster; smaller-scale relative accelerations between individual drifters in a cluster are not considered. While it is impossible to directly determine the relative contribution of each term, the total forcing can be directly estimated as the Lagrangian acceleration is a total derivative of velocity. *Haller et al.* [2002] show that the nonlinear terms in an Eulerian frame are of comparable magnitude to the radiation stress gradient and setup gradient in a laboratory rip channel. Obtaining the spatial gradients of Eulerian velocity required to evaluate the nonlinear terms is difficult in the field as a high sensor density is required.

[43] The accelerations of the clusters were calculated from the second-order centered differences of the centroid position and is shown for the neck region of the four rip events in Figure 15. Both cross-shore and longshore components of acceleration continually change direction indicating oscillatory forcing. This is presumably caused both by variable wave forcing, which leads to an imbalance between the short wave forcing and setup gradient and by surface elevation gradients associated with free infragravity waves. The wave field shows significant groupiness (Figure 7) during the rip events, especially in RE3a and

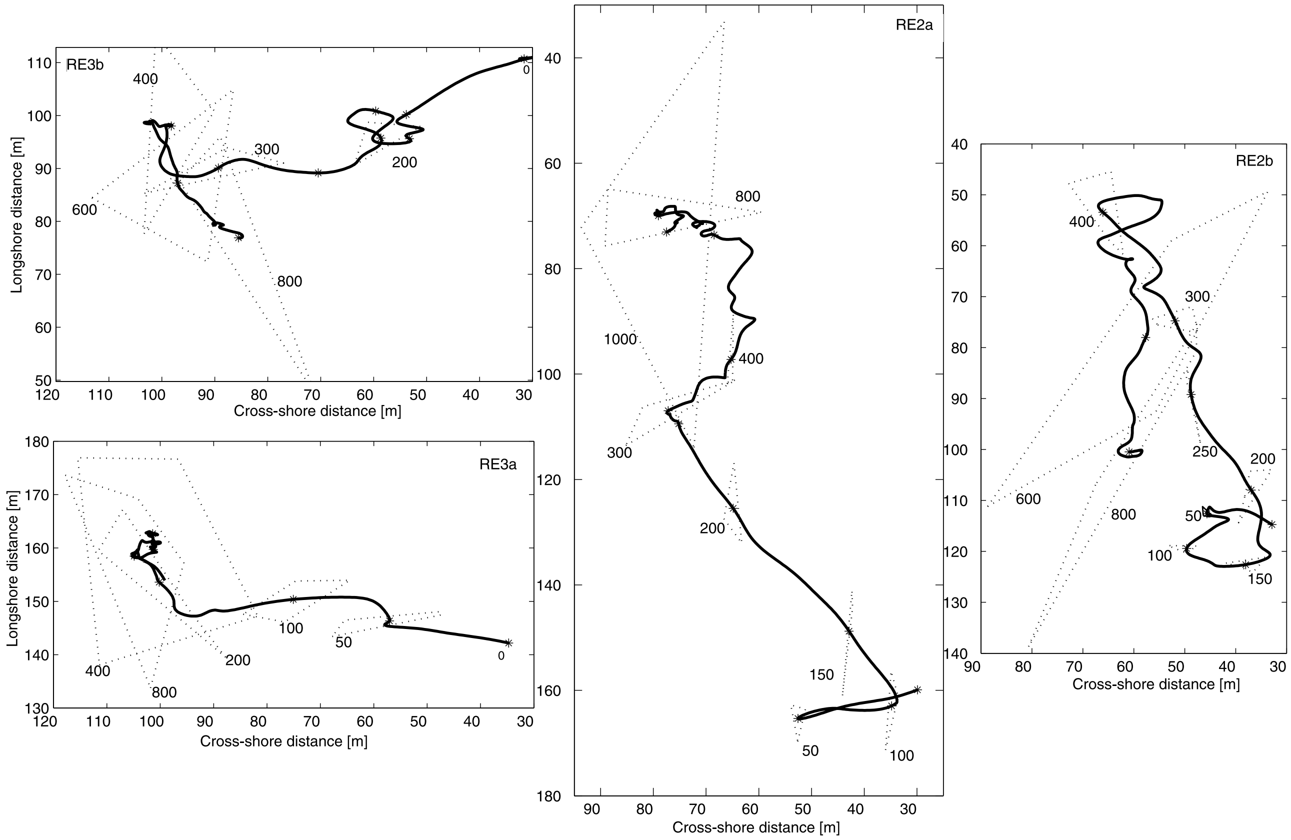

Figure 13. Trajectory of the cluster centroids and area spanned by the cluster for the four rip events. The polygons vertices are formed by the individual drifters. The number by each cluster polygon is the time in seconds since the start of the deployment.

RE3b. The rip current records are unfortunately too short to demonstrate dependence of the acceleration on the short wave envelope with any statistical certainty. Another source of the fluctuations observed in the rip flows may be self-instability. *Haller and Dalrymple* [2001] have investigated this phenomena for laboratory generated topographic rip currents and find that it explains much of the variability of the rip current velocities. The meandering in the latter section of the rip neck in RE2a (Figure 10b) and RE2b (Figure 11b) suggests an instability mechanism. Means, minimums, maximums and standard deviation of the cluster accelerations in the rip neck region are summarized in Table 3.

[44] A conceptual model for the transient rips is of a slow evolution (over the order of hundreds of seconds) of a forced jet-like flow which is then modulated by higher-frequency wave group forcing, infragravity waves and self-instability of the flow. Substantial momentum is input at the start of the rip neck, and this must be sufficient to generate a rip, as temporally variable forcing appears to occur continuously, but transient rip development occurs sporadically at variable locations. As the drifters traverse the rip neck, there appears to be subsequent accelerations of the rip flow as seaward motion is retarded and then resumed. How much of the stop-start behavior is caused by large modulations due to infragravity waves and how much is caused by changes in the underlying rip flow is impossible to ascertain from the data. Similarly, it is not clear what is responsible for the longshore accelerations which cause changes of direction seen in RE2a and RE2b. The eventual deceleration of the neck section of the rips outside the surf zone must be partially caused by bottom friction and lateral mixing.

5.2. Cluster Dispersion

[45] Following *List et al.* [1990], the variance of the drifter positions with respect to the cluster centroid is

$$\sigma_x^2(t) = \frac{\sum_{i=1}^{n}[x_i(t) - x_o(t)]^2}{n-1} \qquad \sigma_y^2(t) = \frac{\sum_{i=1}^{n}[y_i(t) - y_o(t)]^2}{n-1}, \quad (5)$$

where n is the number of drifters. The total dispersion of the drifter clusters can then be expressed as

$$\sigma^2(t) = \frac{\sigma_x^2(t) + \sigma_y^2(t)}{2}. \quad (6)$$

[46] The calculated values of σ, σ_x, and σ_y are shown in Figure 16. A relative dispersion coefficient can be defined by

$$K(t) = \frac{1}{2}\frac{\partial\sigma^2(t)}{\partial t}, \quad (7)$$

which can be approximated directly from the values of σ^2. Directionally dependent values, K_x and K_y can be calculated from σ_x and σ_y respectively.

[47] The clusters in each case show little or no spreading of the cluster within the rip neck region followed a period of expansion in the head region. It is useful to

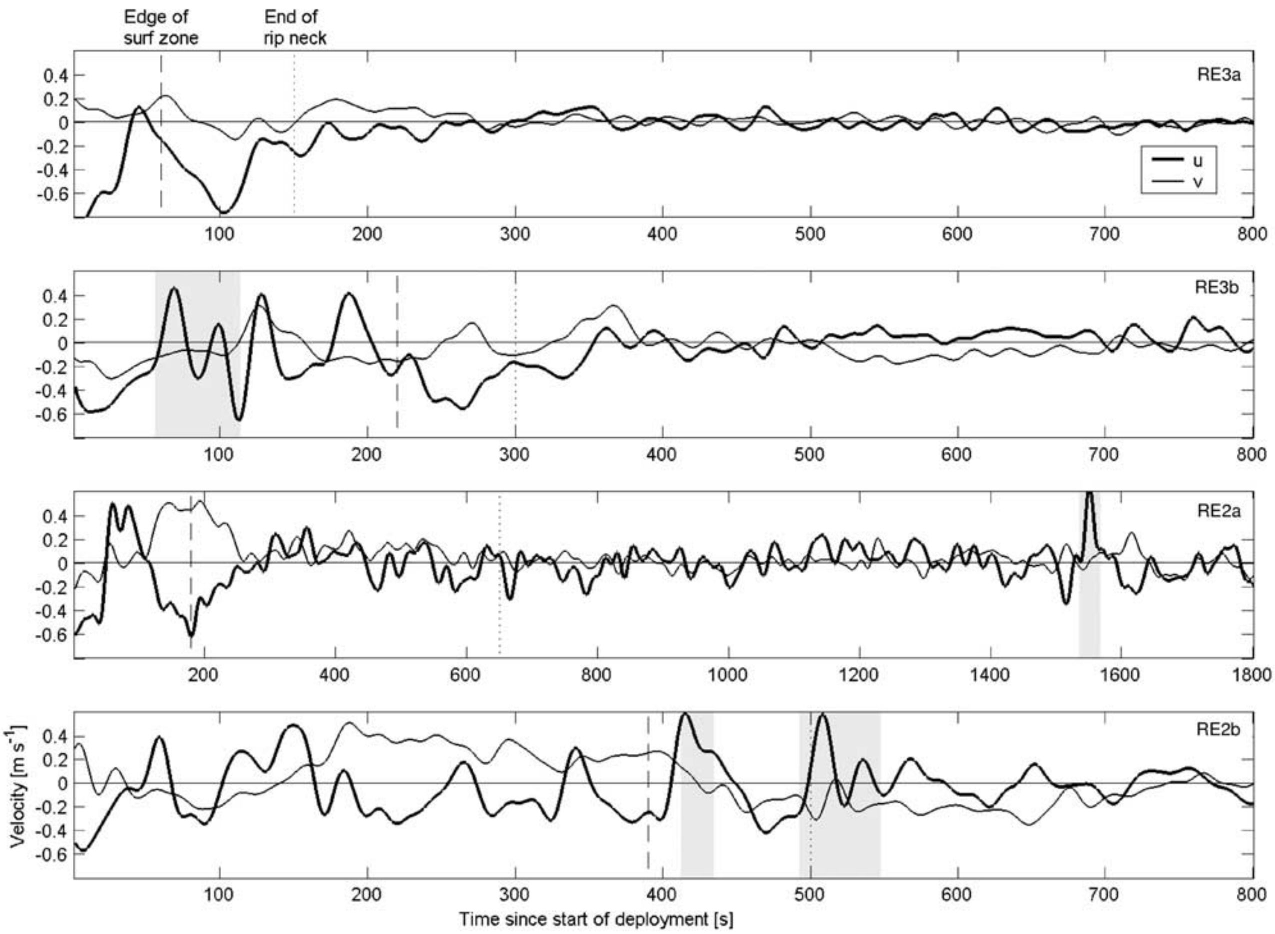

Figure 14. Velocity of the cluster centroid for the four rip events. The shaded regions mark periods in the data affected by the surfing of one or more of the drifters. Note that the time series RE2a is longer than the others.

estimate the dispersion in the head region. To obtain an approximate values for these numbers the gradients of the best fit lines to the dispersion values during the head expansion are used. The period of head expansion is defined as being from the end of the rip neck to the first main peak of the total dispersion. These lines and the respective values of K, K_x, K_y are shown in Figure 16. Although somewhat ad hoc, this gives an estimation of the dispersion in the rip head region, and is a bulk estimate calculated in a similar manner to the surf zone dispersion experiments with dye by *Inman et al.* [1971]. In each case the longshore component of the dispersion coefficient is larger than the cross-shore during expansion of the rip head. The total dispersion values, K, are between 1.29 and 3.88 $m^2\ s^{-1}$. These values are similar to those found by *Inman et al.* [1971] for inside the surf zone over similar length scales. Prior to, and following the rip head expansion, dispersion rates are much lower. The presence of the rip head therefore appears, unsurprisingly, to dramatically enhance mixing outside the surf zone. By contrast, the neck region appears to locally suppress horizontal dispersion when compared to the values of *Inman et al.* [1971]. Note, however, that low dispersion rates are implicit in the selection of the four rip events as deployments where the cluster remains together in the rip neck.

[48] The dispersion coefficient is sometimes negative which is partly due to the fact that the data is only a single realization rather than an ensemble average [*List et al.*, 1990]. In addition, [*List et al.*, 1990] also point out that as a cluster moves into deeper water, continuity means that the surface area of a fluid column has to contract. It is also worth pointing out here that the drifters will not measure

Table 2. Summary Statistics of the Cluster Velocities in the Rip Neck[a]

	Cross-Shore, $m\ s^{-1}$				Longshore, $m\ s^{-1}$			
	$\overline{U}$	U_{min}	U_{max}	σ_U	$\overline{V}$	V_{min}	V_{max}	σ_V
RE3a	−0.33	−0.90	0.12	0.27	0.06	−0.15	0.22	0.10
RE3b	−0.20	−0.59	0.46	0.26	−0.06	−0.30	0.31	0.13
RE2a	−0.06	−0.62	0.50	0.23	0.13	−0.22	0.52	0.16
RE2b	−0.07	−0.56	0.58	0.24	0.09	−0.30	0.51	0.22

[a]For the cross-shore component, $\overline{U}$ is the mean over the duration of the rip neck, U_{min} and U_{max} are minimum and maximum values and σ_U is the standard deviation. Corresponding values are shown for the longshore component, V.

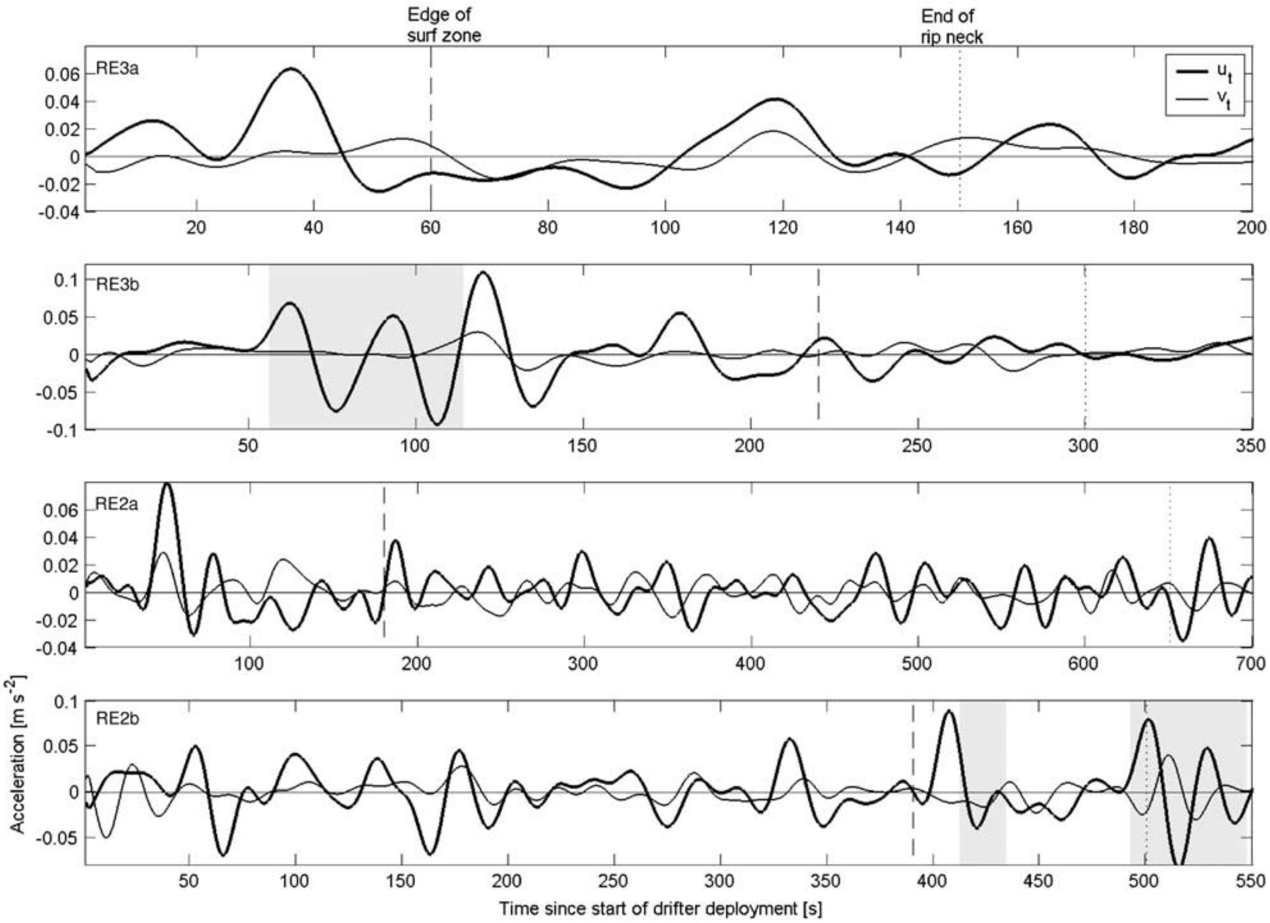

Figure 15. Acceleration of the cluster centroid in the neck region for the four rip events. The shaded regions mark periods in the data affected by the surfing of one or more of the drifters. Note that the time series RE2a is longer than the others.

shear dispersion in the same way as a dye would. This is because they are a connected body spanning the water column and cannot be sheared and mixed vertically like a dye. Much of what *Inman et al.* [1971] were measuring in the cross-shore direction is probably due to such a shear dispersion mechanism, so the results may not be comparable. Note, however, that the momentum mixing mechanism described by *Svendsen and Putrevu* [1994] does affect the drifter trajectories as the shape of the current field, which determines the drifter trajectories, is affected by this mixing.

[49] Values of σ_x, σ_y and the associated K_x, K_y are calculated for the clusters in 14 deployments, including the four considered in detail. There are a total of 13,067 data points, which after filtering corresponds to 653 separate samples. The dispersion values are averaged in 1 m bins of σ_x and σ_y. The dependence of K_x, K_y on σ_x, σ_y for inside and outside the surf zone are plotted in Figure 17 and least squares lines of best fit are calculated for each case. For both inside and outside the surf zone, the longshore dispersion shows a clear power law relationship with the longshore spread of the cluster. There is considerably more scatter in the cross-shore dispersion values and a number of negative values which are not shown in the log plots, however there still appears to be some dependence on the length scale of the cluster. The apparently counter intuitive lower dispersion of the cross-shore component is at least partially explained by the drifters inability to measure shear dispersion. The dispersion is apparently of similar magnitude inside and outside the surf zone when averaged over the whole data set. This is contrary to the relative rip neck/head dispersion seen in the rip events, but is due to the fact that the cluster did not remain together in the rip neck in some of the other rips, and in these cases experiences rapid spreading.

[50] A 4/3 power law relationship for the dispersion, $K = \alpha L^{4/3}$, was first predicted by *Richardson* [1926] (and further explained later by *Batchelor* [1952]) for a pair of particles separated by L in a homogeneous, stationary turbulent flow

Table 3. Summary Statistics of the Cluster Accelerations in the Rip Neck[a]

	Cross-Shore, m s^{-2}				Longshore, m s^{-2}			
$\times 10^{-2}$	$\overline{U_t}$	$U_{t_{\min}}$	$U_{t_{\max}}$	σ_{U_t}	$\overline{V_t}$	$V_{t_{\min}}$	$V_{t_{\max}}$	σ_{V_t}
RE3a	0.41	−2.56	6.35	2.01	−0.05	−1.69	1.82	0.81
RE3b	0.10	−14.9	10.9	3.15	0.10	−2.26	7.62	1.06
RE2a	0.09	−3.54	7.98	1.69	0.03	−1.82	2.90	0.86
RE2b	0.08	−8.36	27.1	3.16	−0.09	−16.1	4.04	1.58

[a]For the cross-shore component, $\overline{U_t}$ is the mean over the duration of the rip neck, $U_{t_{\min}}$ and $U_{t_{\max}}$ are minimum and maximum values and σ_{U_t} is the standard deviation. Corresponding values are shown for the longshore component, V_t.

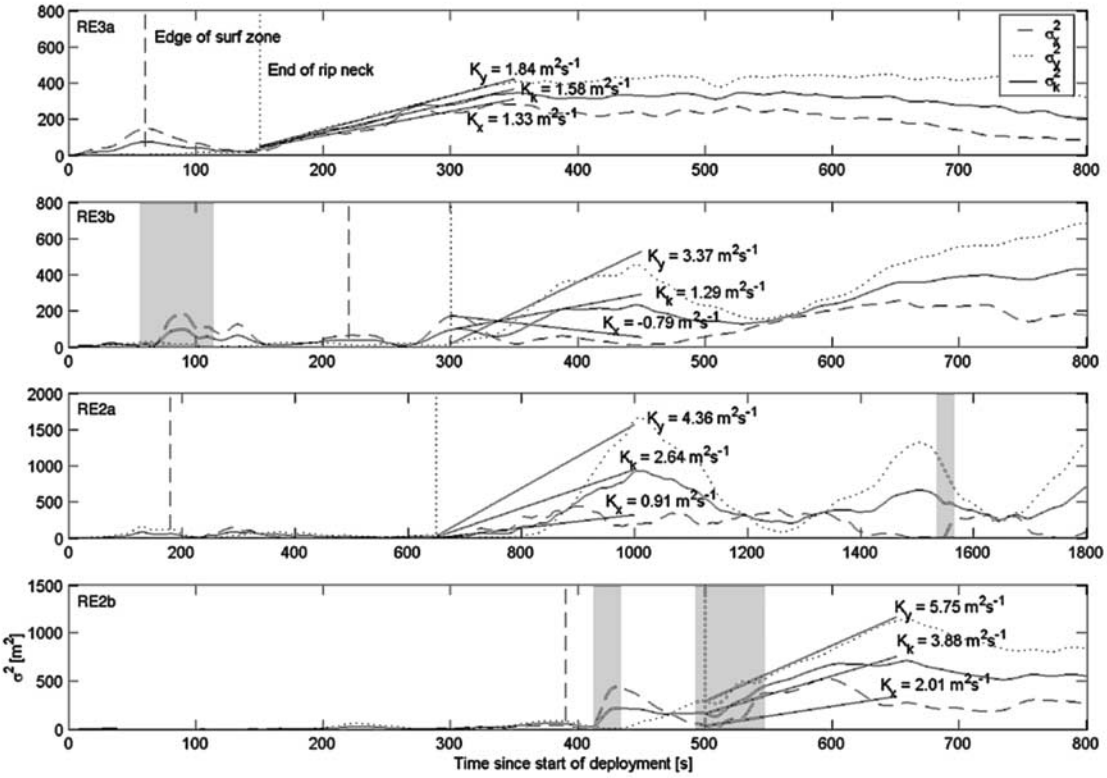

Figure 16. Dispersion of the clusters for the four rip events. The time at which the cluster centroid crosses the approximate location of both the outer edge of the surf zone and the end of the rip neck are shown. Periods where one of the drifters was caught in a surfing event is indicated by the grey shading.

if sufficient time has elapsed that they their positions are independent of their initial separation. However, given that the data here is neither stationary nor homogeneous, is close to a boundary, and that the entire flow field was not sampled uniformly, it is surprising that the dispersion of the clusters should show a power law relationship with an exponent close to 4/3. However, *Okubo* [1974] discusses the fact that other theories of turbulent dispersion lead to the same 4/3 power law result without the rather strict assumptions in the classical analysis of *Batchelor* [1952]. Scale dependence close to the 4/3 relationship is seen over a remarkably large range of scales (1000 km to 10 m) in the ocean [*Okubo*, 1974]. A scale dependence indicates caution is needed when comparing measured dispersion values in the nearshore. For example, values for K of 0.03 m^2 s^{-1} found by *Rodriguez et al.* [1995] compare well with the smaller scales in Figure 17, but are orders of magnitude different for the larger scales. This also implies that when modeling surf zone processes, appropriate diffusion coefficients are dependent on the model grid scale.

6. Spatial Variability of the Current Field

[51] In order to derive quantitative spatial information from Lagrangian data, single or particle pair statistics are normally used to describe the dispersion and velocity correlations. This type of analysis has been used extensively with oceanic drifter data, examples include *Davis* [1985] and *Paduan and Niiler* [1993]. While there have been dye experiments conducted in the surf zone [e.g., *Sonu*, 1972; *Inman et al.*, 1971; *Brander*, 1999], there has been no analysis of drifter field data, that we are aware of, using particle statistics. The calculation of cluster dispersion presented in the last section is equivalent to the rate of particle pair separation. What follows is a first attempt to estimate spatial length scales with Lagrangian trajectories in the nearshore zone.

[52] The velocity covariance of a pair of fluid columns moving with the depth averaged velocity, which, as in section 5.1, we assume is sufficiently well sampled by the drifters, is given by

$$C_{ij}(\mathbf{r},\mathbf{r}') = \left\langle u_i[\mathbf{r}(t_0,\mathbf{r}_0)]\, u_j'\left[\mathbf{r}'\left(t_0,\mathbf{r}_0'\right)\right]\right\rangle, \tag{8}$$

where $\mathbf{r}$ is a displacement vector, and u_i a velocity vector component of a column which started at $\mathbf{r}_0$, primes indicate quantities associated with a second column. The $\langle . \rangle$ indicates ensemble averaging over many particle pair realizations but in practice ergodicity is assumed to allow temporal averaging to be used. The very nature of the experiment has preferentially sampled the rip events which will bias the calculation of C_{ij} so that it describes particular times and longshore locations within the flow field. The amount of data is small for this type of analysis so the results have limited statistical validity. However, useful information can still be gained about typical length scales.

[53] As the rips do not appear to have preferred longshore positions, we assume that C_{ij} is a function of the longshore separation, $y'-y$, rather than absolute position. Dependence

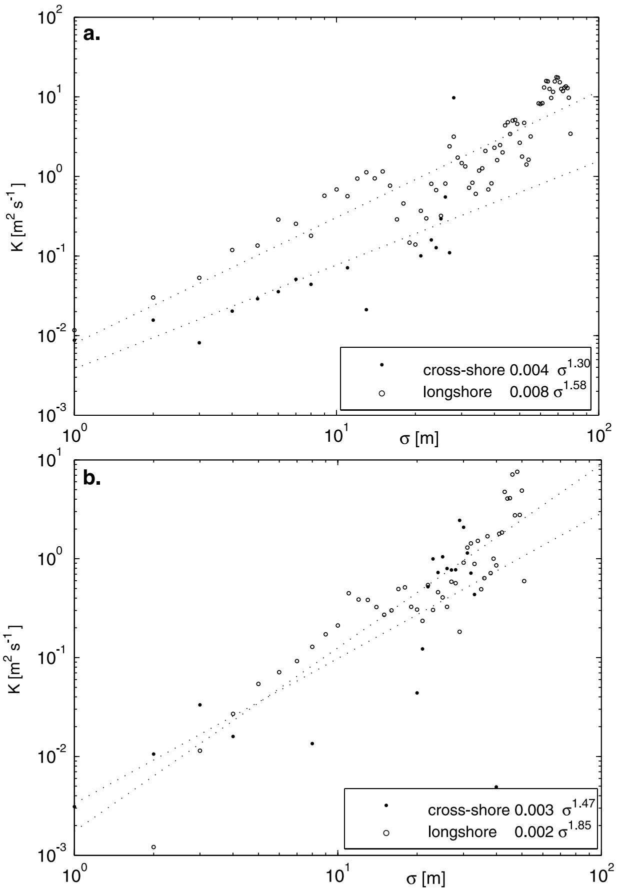

Figure 17. Cross-shore (solid circles) and longshore (open circles) dispersion coefficients averaged in 1 m bins of standard deviation of cross-shore and longshore separation for (a) inside the surf zone and (b) outside the surf zone. The line shown are the least squares fit, and the equation of each line is shown in the legends.

on cross-shore location is retained as the flow field is expected to be nonhomogeneous across the surf zone. Following the method of *Davis* [1985], the mean current and the covariance of observation pairs are averaged in discrete spatial bins which is equivalent to the covariance of a velocity which has been spatially filtered with a low-pass cutoff of the same size as the averaging bins (for a proof see appendix by *Davis* [1985]). Bins of 5 m are used for the cross-shore position and for the longshore separation. The covariance estimate, $\tilde{C}_{ij}(\zeta_1, \zeta_2, \xi)$, is the average covariance calculated for all pairs of simultaneous observations with cross-shore locations in bins centered at ζ_1 and ζ_2 and with longshore separation in the bin with center at ξ.

[54] The longshore covariance function, $L_{ij}(y)$ for each cross-shore zone spanning x_1 to x_2 of

$$L_{ij}(y; x_1, x_2) = \frac{\sum_n \tilde{C}_{ij}(x_n, x_n, y) N(x_n, x_n, y)}{\sum_n N(x_n, x_n, y)}; \qquad x_1 <= x_n < x_2, \tag{9}$$

where N is the number of pairs in each covariance estimate. Because the quantity of data in some of the longshore separation bins is small, $L_{ij}(y; x_1, x_2)$ is also smoothed with a 1-2-1 kernel. Smoothed longshore covariance functions for cross-shore zones of x_1 = 35 m to x_2 = 65 m (inside the surf zone) and x_1 = 65 m to x_2 = 95 m (outside the surf zone) are calculated and normalized by $L_{ij}(0; x_1, x_2)$. The covariance of velocities with cross-shore separation from a particular cross-shore location, x_c give a cross-shore covariance function, $M_{ij}(|x - x_c|; x_c)$:

$$M_{ij}(|x - x_c|; x_c) = \frac{\tilde{C}_{ij}(x_c, x_c + x, 0)N(x_c, x_c + x, 0) + \tilde{C}_{ij}(x_c, x_c - x, 0)N(x_c, x_c - x, 0)}{N(x_c, x_c + x, 0) + N(x_c, x_c - x, 0)}. \tag{10}$$

The cross-shore covariance functions are calculated for x_c = 50 m and x_c = 70 m, then smoothed with a 1-2-1 kernel and normalized by $M_{ij}(0; x_c)$.

[55] Correlation functions calculated separately for nine deployments from experiment 1 and experiment 3 and five deployments from experiment 2 in view of the different type of rip flows observed; results are shown in Figure 18. The limited amount of data means some of the curves have somewhat unusual shapes and caution is required in how much can be reliably determined from the results. It is important to realize that the structure of the correlation functions will be partially determined by infragravity motion. However, the sampling bias of times and locations where transient rips were occurring means that the displacement at which the correlation falls to zero is useful as a reasonable estimate of length scales of the rip flows.

[56] Data from experiments 1 and 3 show a longshore decorrelation length scale of around 20–30 m. This is consistent with the observation in section 4.1 of a significant difference between drifter velocities and ADCP data 20 m alongshore. The decorrelation length in the cross-shore direction is slightly longer at around 30–40 m, which would be expected for a cross-shore jet type flow. The decorrelation lengths from inside and outside of the surf zone are similar. The curves for experiment 2 show similar length scales to experiments 1 and 3, but in the opposite sense with longshore scales of 30–40 m and cross-shore scales of 20–30 m; this would be expected as the rips were oriented obliquely to the shore. Again in this case, inside and outside of the surf zone are similar in terms of decorrelation lengths. The fact that short cross-shore scales are somewhat shorter than the width of the surf zone in experiment 2 (RE2a and RE2b) indicate that the flow is a jet-like flow as opposed to a continuous (across the surf zone) longshore flow. The strong negative cross-shore correlations of $\langle vv \rangle$ in experiment 2 (Figure 18c) appear because of "oversampling" of pairs of drifters moving in opposite longshore directions at the end of the rip necks. This is an artifact of the small number of data and the sampling of a small number of individual rip current events. Given the limitations of the data it is hard to draw any conclusions regarding the difference between $\langle uu \rangle$ and $\langle vv \rangle$ correlation estimates.

7. Discussion

[57] The data shown in Figure 5 shows that the long time average of depth averaged velocity is close to zero in both the longshore and cross-shore direction. This is what would

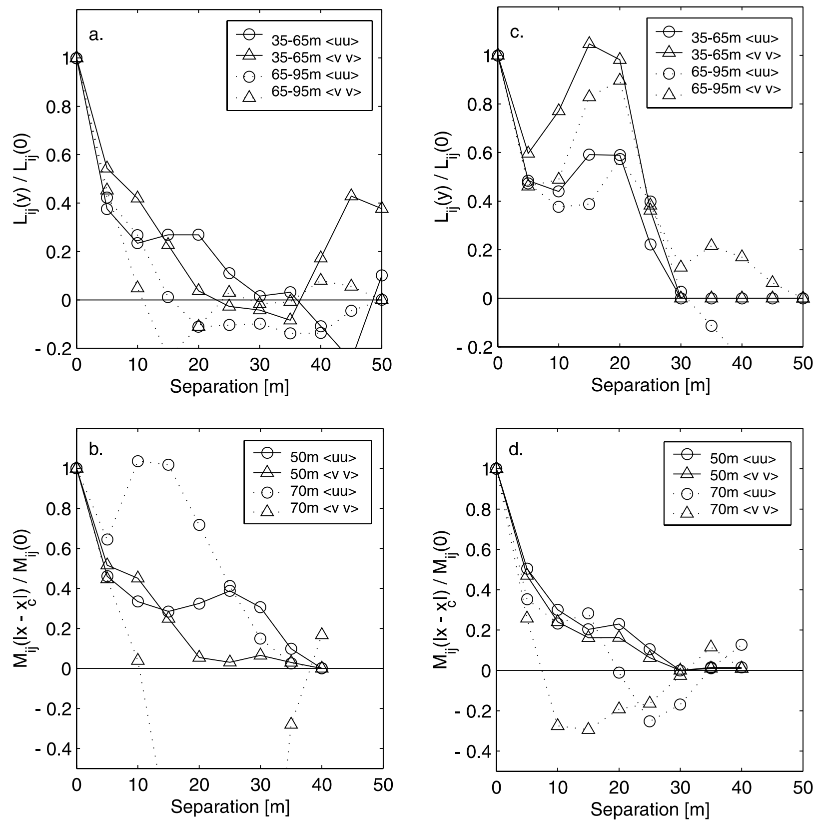

Figure 18. Spatial correlations calculated from all deployments. (a) Longshore correlation for experiments 1 and 3. (b) Cross-shore correlation for experiments 1 and 3. (c) Longshore correlation for experiment 2. (d) Cross-shore correlation for experiment 2. Longshore correlations are for cross-shore zones of x_1 = 35 m to x_2 = 65 m (solid line; inside the surf zone) and x_1 = 65 m to x_2 = 95 m (dashed line; outside the surf zone). Cross-shore covariance functions $M_{ij}(|x - x_c|)$ are normalized by $M_{ij}(0)$ for cross-shore reference positions, x_c, of 50 m (solid line; inside the surf zone) and 70 m (dashed line; outside the surf zone). In Figure 18b the section of the axis below -0.5 is omitted to retain clarity in the positive half; the correlation reaches a minimum of -3.0 at a cross-shore separation of 25 m.

be expected for the experimental conditions with waves perpendicular to a longshore uniform beach. However, what the drifter trajectories have also shown is an active varying horizontal circulation which occurs over timescales greater than the incident wave period. Much of the fluctuations in the trajectories will be due to infragravity waves, which are the dominant source of the total current variance. However, there is separate part of the velocity field associated with another type of motion as indicated by the energy ratios calculated in section 3. The noninfragravity flow mode must be rotational and nondivergent, as are shear waves. The tendency of nearshore flows on beaches with gentle slopes to be two-dimensional, rotational and contain discrete eddies has been highlighted by *Peregrine* [1998], who also discusses how random breaking waves can generate vorticity even with a mean perpendicular incidence on a longshore uniform beach. Given the lack of longshore current, the variable rotational flow measured here does not derive its vorticity from the longshore current shear, and cannot be classified as shear waves. Rather, this rotational flow mode could be thought of as ‘‘infragravity turbulence’’, with vorticity introduced by the spatial variability of a random incident wave field, and which includes discrete vortices and transient rips seen in the drifter trajectories.

[58] It seems likely that discrete vortex features are important in the rip generation mechanism. In their drifter measurements of a rip current reoccurring in the same location (and therefore presumably topographic), *Schmidt et al.* [2003] show the presence of a persistent eddy within the surf zone at the shoreward end of offshore flow in the rip neck. Numerical experiments of topographic rips [*Haas et al.*, 2001; *Chen et al.*, 1999] clearly show the generation and subsequent shedding of vortex pairs from the edges of the rip channels. Despite the lack of a bar with rip channels, the start of the deployment shown in RE2b (Figure 12) clearly shows a vortex feature which appears similar to this type of starting vortex. Although the rip itself is somewhat oblique to the shore this suggests the initial stages of transient rip flow may be similar in that a vortex is involved at the landward (inlet) end. *Buhler and Jacobson* [2001] point out that transient rips could in principle be generated through the formation of counter rotating vortex pairs which propagate offshore. *Buhler and Jacobson* [2001] also point out that single vortices with opposite rotations will tend to propagate longshore, collide and form a vortex pair; thus generation of a vortex pair during a particular forcing event itself may not be necessary. Upscale evolution of vortex energy, inherent to two-dimensional turbulence, may also lead to vortices large

enough to produce a rip current being generated through the merging of smaller vortices. Infragravity waves will modulate the relative vorticity of vortices by vortex stretching, which may cause a pumping mechanism which enhances offshore propagation. Lagrangian data provides a means to resolve discrete surf zone current eddies in the field and further investigation should lead to a better understanding of the evolution of eddies and their role in rip current formation.

[59] It is not possible to conclusively prove that the circulation in the data are not topographically controlled as a complete bathymetry for the field site is not available; the evidence here is somewhat circumstantial. However, Boussinesq modeling of circulation on a plane beach of the same slope and with a similar random wave field shows the development of complex circulation and narrow offshore jets at the same scales as the rips described in this paper. These results, which will be presented elsewhere, are further evidence that this type of circulation does not need to be topographically controlled.

8. Summary and Conclusions

[60] Measurements using Lagrangian and Eulerian techniques on a swell-dominated beach show a complex nearshore current field. Estimates of energy ratios using the method of *Lippmann et al.* [1999] show that while the infragravity wave energy is dominant, there is a significant variable component of the current field not related to infragravity motion. One well-defined feature of this variable noninfragravity current field is the ejection of transient rip currents from inside the surf zone. Lagrangian measurements reveal the following characteristics of the rip dynamics:

[61] 1. Substantial momentum is imparted to the rip flow at the start of the rip neck.

[62] 2. There is continuous modulation of the current field at infragravity wave frequencies.

[63] 3. The rip neck region is constrained and has short (20–30 m) length scales across the main axis of the flow.

[64] 4. The rip head appears to be a region of enhanced mixing with relative dispersion coefficients between 1.29 and 3.88 $m^2 s^{-1}$.

[65] 5. Discrete vortices are seen both at the initiation of one of the rips and in the rip head region of another.

[66] The estimates of dispersion indicate that transient rips should greatly enhance mixing in the region outside the surf zone. An evaluation of all of the data appears to show scale dependence with best fit power laws ranging between 1.30 and 1.85. The existence of a predictable scale dependence has some very useful implications for modeling nearshore dispersion of material. Further investigation is desirable to see if this is ubiquitous in the nearshore.

[67] **Acknowledgments.** The authors wish to thank A. Berthot, D. Byrne and K. Judge for assistance during the field work. This work was carried out while D. Johnson was in receipt of a University Postgraduate Award (International) from the University of Western Australia. This is contribution ED1771 from the Centre for Water Research, University of Western Australia. We are grateful for the helpful comments and suggestions of the anonymous reviewers. We would especially like to thank S. M. Henderson for valuable discussion about this work.

References

Aagaard, T., B. Greenwood, and J. Nielsen (1997), Mean currents and sediment transport in a rip channel, *Mar. Geol.*, *140*, 25–45.

Allen, J., P. Newberger, and R. Holman (1996), Nonlinear shear instabilities of alongshore currents on plane beaches, *J. Fluid Mech.*, *310*, 181–213.

Batchelor, G. (1952), Diffusion in a field of homogeneous turbulence. II. The relative motion of particles, *Proc. Cambridge Philos. Soc.*, *48*, 345–363.

Bowen, A. (1969), Rip currents: 1. Theoretical investigations, *J. Geophys. Res.*, *74*, 5479–5490.

Bowman, D., D. Arad, D. Rosen, E. Kit, R. Goldbery, and A. Slavicz (1988a), Flow characteristics along the rip current system under low energy conditions, *Mar. Geol.*, *82*, 149–167.

Bowman, D., D. Rosen, E. Kit, D. Arad, and A. Slavicz (1988), Flow characteristics at the rip current neck under low energy conditions, *Mar. Geol.*, *79*, 41–54.

Brander, R. (1999), Field observations on the morphodynamic evolution of a low-energy rip current system, *Mar. Geol.*, *157*, 199–217.

Brander, R., and A. Short (2000), Morphodynamics of a large-scale rip current system at Muriwai Beach, New Zealand, *Mar. Geol.*, *165*, 27–39.

Buhler, O., and T. Jacobson (2001), Wave-driven currents and vortex dynamics on barred beaches, *J. Fluid. Mech.*, *449*, 313–339.

Chen, Q., R. Dalrymple, J. Kirby, A. Kennedy, and M. Haller (1999), Boussinesq modelling of a rip current system, *J. Geophys. Res.*, *104*, 20,617–20,637.

Cook, D. (1969), The occurrence and geological work of rip currents off southern California, *Mar. Geol.*, *9*, 173–186.

Dalrymple, R. (1975), A mechanism for rip current generation on an open coast, *J. Geophys. Res.*, *80*, 3485–3487.

Dalrymple, R., and C. Lozano (1978), Wave current interaction models for rip currents, *J. Geophys. Res.*, *83*, 6063–6071.

Davis, R. (1985), Drifter observations of coastal surface currents during code: The statistical and dynamical views, *J. Geophys. Res.*, *90*, 4756–4772.

Fowler, R., and R. Dalrymple (1991), Wave group forced nearshore circulation, paper presented at 22nd International Conference on Coastal Engineering, Am. Soc. of Civ. Eng., Delft, Netherlands.

Haas, K., I. Svendsen, and M. Haller (1999), Numerical modelling of nearshore circulation on a barred beach with rip channels, in *Coastal Engineering 1998*, edited by B. L. Edge, pp. 801–814, Am. Soc. of Civ. Eng., Reston, Va.

Haas, K., I. Svendsen, and Q. Zhao (2001), 3-D modelling of rip currents, paper presented at 27th International Conference on Coastal Engineering, Am. Soc. of Civ. Eng., Sydney, Australia.

Haller, M., and R. Dalrymple (2001), Rip current instabilities, *J. Fluid Mech.*, *433*, 161–192.

Haller, M., R. Dalrymple, and I. Svendsen (2002), Experimental study of nearshore dynamics on a barred beach with rip channels, *J. Geophys. Res.*, *107*, 3061, doi:10.1029/2001JC000955.

Hino, M. (1975), Theory on the formation of rip current and cuspidal coast, paper presented at 14th International Conference on Coastal Engineering, Am. Soc. of Civ. Eng., Copenhagen.

Huntley, D., and A. Short (1992), On the spacing between observed rip currents, *Coastal Eng.*, *07*, 211–225.

Inman, D., R. Tait, and C. Nordstrom (1971), Mixing in the surf zone, *J. Geophys. Res.*, *76*, 3493–3514.

Johnson, D., and C. Pattiaratchi (2003), Surfzone drifters, *CWR Rep. ED 1770 DJ*, Cent. for Water Res., Univ. of West. Aust., Perth.

Johnson, D., R. Stocker, R. Head, J. Imberger, and C. Pattiaratchi (2004), A compact, low-cost GPS drifter for use in the oceanic nearshore zone, lakes and estuaries, *J. Atmos. Oceanic Technol.*, *20*, 1880–1884.

LeBlond, P., and C. Tang (1974), On energy coupling between waves and rip currents, *J. Geophys. Res.*, *79*, 811–816.

Lippmann, T., T. Herbers, and E. Thornton (1999), Gravity and shear wave contributions to nearshore infragravity motions, *J. Phys. Oceanogr.*, *29*, 231–239.

List, E., G. Gartrell, and C. Winant (1990), Diffusion and dispersion in coastal waters, *J. Hydraul. Eng.*, *116*, 1158–1179.

Masselink, G., and C. Pattiaratchi (2002), Seasonal variation in nearshore processes and beach morphology along the sheltered coastline of Perth, Western Australia, *Mar. Geol.*, *172*, 242–263.

Murray, A., and G. Reydellet (2002), A rip current model based on a hypothesized wave/current interaction, *J. Coastal Res.*, *17*, 517–530.

Murray, A., M. LeBars, and C. Guillon (2004), Tests of a new hypothesis for non-bathymetrically driven rip currents, *J. Coastal Res.*, *19*, 269–277.

Noyes, J., R. Guza, S. Elgar, and T. Herbers (2002), Comparison of methods for estimating nearshore shear wave variance, *J. Atmos. Oceanic Technol.*, *19*, 136–143.

Okubo, A. (1974), Some speculations on oceanic diffusion diagrams, *Rapp. P. V. Reun. Cons. Int. Explor. Mer*, *167*, 77–85.

Ozkan-Haller, H., and J. Kirby (1999), Nonlinear evolution of shear instabilities of the longshore current: A comparison of observations and computations, *J. Geophys. Res.*, *104*, 25,953–25,984.

Paduan, J., and P. Niiler (1993), Structure of velocity and temperature in the northeast Pacific as measured with Lagrangian drifters in fall 1987, *J. Phys. Oceanogr.*, *23*, 585–600.
Peregrine, D. (1998), Surf zone currents, *Theor. Comput. Fluid Dyn.*, *10*, 295–309.
Richardson, L. (1926), Atmospheric diffusion shown on a distance-neighbour graph, *Proc. R. Soc. London, Ser. A*, *110*, 709–727.
Rodriguez, A., A. A. Snchez-Arcilla, J. Redondo, E. Bahia, and J. Sierra (1995), Pollutant dispersion in the nearshore region: Modelling and measurements, *Water Sci. Technol.*, *32*, 169–178.
Sasaki, T., and K. Horikawa (1975), Nearshore current system on a gently sloping bottom, *Coastal Eng. Jpn.*, *18*, 123–142.
Sasaki, T., and K. Horikawa (1978), Observation of nearshore current and edge waves, in *Coastal Engineering 1978*, pp. 791–809, Am. Soc. of Civ. Eng., Reston, Va.
Schmidt, W., B. Woodward, K. Millikan, R. Guza, B. Raubenheimer, and S. Elgar (2003), A GPS-tracked surf zone drifter, *J. Atmos. Oceanic Technol.*, *20*, 1069–1075.
Shepard, F., and D. Inman (1950), Nearshore water circulation related to bottom topography and wave refraction, *Eos Trans. AGU*, *31*, 196–213.
Shepard, F., K. Emery, and E. LaFond (1941), Rip currents: A process of geological importance, *J. Geol.*, *49*, 337–369.
Short, A. (1985), Rip-current spacing and persistence, Narrabeen Beach, Australia, *Mar. Geol.*, *65*, 47–71.
Smith, J., and J. Largier (1995), Observations of nearshore circulation: Rip currents, *J. Geophys. Res.*, *100*, 10,967–10,975.
Sonu, C. (1972), Field observations of nearshore circulation and meandering currents, *J. Geophys. Res.*, *77*, 3232–3247.
Svendsen, I., and U. Putrevu (1994), Nearshore mixing and dispersion, *Proc. R. Soc. London, Ser. A*, *545*, 561–576.
Svendsen, I., K. Haas, and Q. Zhao (2001), Analysis of rip current systems, paper presented at 27th International Conference on Coastal Engineering, Am. Soc. of Civ. Eng., Sydney, Australia.
Symonds, G., and R. Ranasinghe (2001), On the formation of rip currents on a plane beach, paper presented at 27th International Conference on Coastal Engineering, Am. Soc. of Civ. Eng., Sydney, Australia.
Symonds, G., R. Holman, and B. Bruno (1998), Rip currents, in *Coastal Dynamics '97*, edited by E. Thornton, pp. 584–593, Am. Soc. of Civ. Eng.
Tang, E.-S., and R. Dalrymple (1989), *Nearshore Circulation: Rip Currents and Wave Groups*, edited by R. J. Seymour, Plenum, New York.
Vos, R. (1976), Observations on the formation and location of transient rip currents, *Sediment. Geol.*, *16*, 15–19.

D. Johnson and C. Pattiaratchi, Centre for Water Research, University of Western Australia, 35 Stirling Highway, Perth, Western Australia 6009, Australia. (johnson@cwr.uwa.edu.au)